Deployment Dynamics Analysis of an Origami-Folded Spacecraft Structure with Elastic Hinges

JoAnna Fulton* and Hanspeter Schaub†
University of Colorado Boulder, Boulder, Colorado 80303-0429

Self-actuated deployable space structures present a novel challenge for deployment dynamics modeling efforts, where the system-level influence of strain energy components must be captured. Here, the free deployment of an origami-folded structure through actuation of strain energy hinges is studied. Studies include experimental testing, multibody dynamics modeling, and finite element modeling. An approach for modeling high strain tape spring hinges for use in a multibody simulation of free-deployment dynamics analysis is presented and demonstrated. This approach considers hinges with multiple degrees of freedom beyond the primary fold axis angle. A novel folded deployable structure is designed and prototyped with a segmented fold pattern and strain energy hinges integrated in the design. A suite of deployment tests is conducted on the prototype using videogrammetry. A full simulation of the prototype is constructed from a multibody dynamics model and the hinge model, and the predicted deployment behavior for relative hinge states is evaluated against the experimental testing. Additionally, the prototype deployment is replicated using an explicit dynamic finite element analysis for a performance comparison. The models demonstrate strong correlation for deployment time predictions across the relative hinge states, and the finite element analysis correlates all deployment behaviors.

Nomenclature

$\mathcal{A}_i$	=	tape spring reference frame
a_i	=	polynomial coefficient
$\hat{\boldsymbol{a}}_{0_i}$	=	reference frame unit vector
$b_{j,k}$	=	polynomial coefficient
c_i	=	polynomial coefficient
$\boldsymbol{f}_i$	=	generalized spatial force, N
$\mathcal{H}_i$	=	hinge frame
$\boldsymbol{M}_i$	=	moment at frame i, N/mm
$\boldsymbol{N}_i$	=	force at frame i, N
$\mathcal{P}_i$	=	panel frame
$p(\boldsymbol{q})$	=	polynomial function
$\hat{\boldsymbol{p}}_{i,j}$	=	reference frame unit vector
$\boldsymbol{q}$	=	generalized spatial coordinates
$\boldsymbol{r}_i$	=	global position vector, mm
$\boldsymbol{\delta}$	=	relative position vector, mm
δ_i	=	relative position coordinate, mm
ϵ	=	numerical buffer
$\boldsymbol{\theta}$	=	orientation coordinates, deg
θ_i	=	Euler angle, deg
σ_i	=	spacecraft modified Rodrigues parameters' attitude orientations
ω_i	=	spacecraft rotation rates, deg/s

Subscripts

i	=	variable index
j	=	variable index
k	=	variable index

*Graduate Research Assistant, Aerospace Engineering Sciences, Colorado Center for Astrodynamics Research, 3775 Discover Drive, 429 UCB. Student Member AIAA.

†Glenn L. Murphy Chair of Engineering, Aerospace Engineering Sciences, Colorado Center for Astrodynamics Research, 3775 Discover Drive, 429 UCB. Associate Fellow AIAA.

I. Introduction

AN EMERGING area in the deployable space structures field is known as origami structures and takes primary inspiration from origami-folding techniques. These are developed to stow flat structures with a large area to size ratio relative to the spacecraft bus, such as solar [1–3] and phase [4,5] arrays, star occulters [6], and reflector antennas [7,8]. Concept imagery is shown for two solar array designs in Fig. 1, where the Alliant Techsystems (ATK) design uses a cable and motor system to actuate deployment and the Brigham Young University (BYU) design uses an external perimeter truss and cable system [9].‡,§

Adapting origami-folding techniques to space structures requires either creasing or segmentation of the structure surface. Creasing primarily applies to pliable membrane structures, and the challenges of membrane creasing have been [10] and continue to be [11] researched in the literature. The scope of this paper focuses on rigid or semirigid segmented structures, meaning the individual segmented panels of the structure can be treated as rigid or semirigid with respect to the mobility of the folds.

A central challenge for origami structures includes the deployment dynamics and deployment actuation of the folded structure and spacecraft system. A novel lightweight solution for deployment actuation is to integrate strain energy hinges that can also facilitate folding [12]. Elastic, flexible hinges are ideal for this application because they provide an intuitive lightweight solution to traditional mechanical hinges. Traditional hinges such as the pin/clevis rotation joints are mechanically complex and massive. An elastic hinge, such as a composite or metallic shell, has the potential to reduce mass, eliminate friction loss, and increase compaction. Additionally, elastically folding materials will store strain energy in the system, providing a built-in deployment actuator. This enables a free-deploying structure design, meaning the deployment is not controlled electronically by a motor actuation system.

Deployment dynamics of such a system would typically be simulated through finite element analysis (FEA) [13]. However, for a structure with multiple high strain hinges, FEA modeling would require significant computational time and skill because these hinges

‡"ATK Demonstrates High-Power MegaFlex Solar Array for NASA," ATK, 2014, http://photos.prnewswire.com/prnh/20140121/CG49597 [retrieved 14 April 2020].

§"Origami in Space: BYU-Designed Solar Arrays Inspired by Origami," Brigham Young Univ., Provo, UT, 2013, https://www.youtube.com/watch?v=3E12uju1vgQ [retrieved 14 April 2020].

a) ATK megaflex [10]   b) BYU design [11]
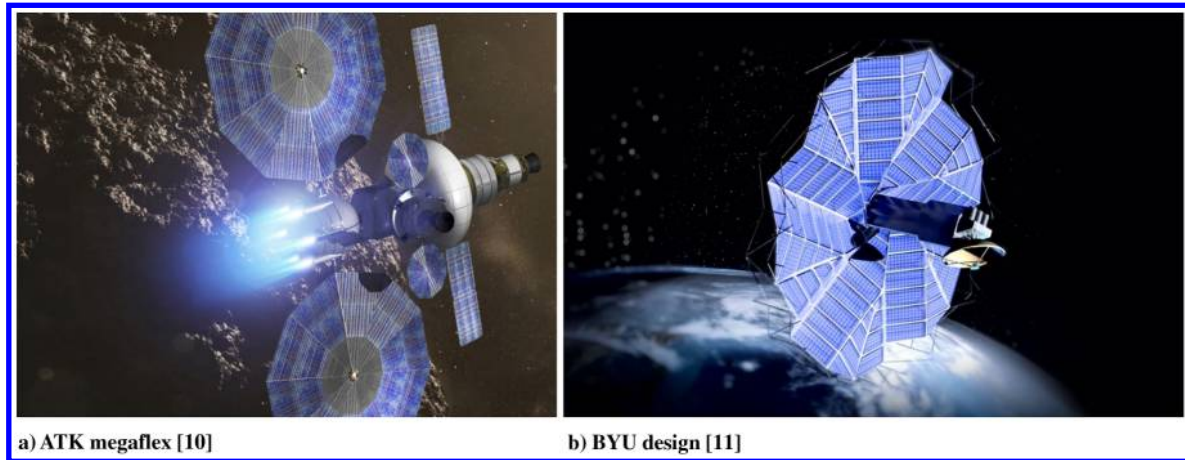
Fig. 1   Folded deployable spacecraft structure solar array concept art.

exhibit large deformations of shell structures with nonlinear behavior. This limits the ability to explore parameter design spaces and iterate toward more optimal solutions. An alternative method for studying the system dynamics that uses multibody dynamics and a simplified hinge representation would provide significant gains in computation time [14,15]; however, this method still requires adequate skill and experience. In this approach, fold panels are treated as rigid bodies and the flexible joints are represented by internal forcing functions. In this paper, a model to represent the hinge mechanics is designed as a function of the hinge's multiple degrees of freedom, as defined by the relative position and orientation states across the hinge [16]. This model is designed to be implemented in a multibody dynamics algorithm developed specifically for origami-folded deployable spacecraft structures [17]. The methodology aims to provide a deployment dynamics behavior approximation without a full FEA simulation of the system. The results show that the deployment phase behavior and deployment time are well modeled but settling behaviors are not due to the absence of damping or contact.

The paper is organized as follows. A multibody dynamics model and a flexible hinge model are integrated to provide a complete deployable structure model based on a prototype structure. The approach to developing the high strain tape spring hinge descriptions is designed for direct use in multibody dynamics algorithms. First, a simulation of the prototype case is developed under the assumption that the elastic tape spring hinges are operating on a single degree of freedom. A single-degree-of-freedom hinge model is developed by fitting torque response data from experiments for the symmetric fold case. Following this, the full six-degree-of-freedom hinge case is built. A deployment test campaign is conducted on the prototype structure to provide experimental comparison data for the simulations. An additional deployment dynamics simulation is studied using FEA to further validate the results and provide context for performance and expectations of the multibody model. The literature lacks demonstration of FEA modeling for folding deployable structures, and therefore this study provides insights for the greater community on its relative use and performance with respect to a multibody model. Additionally, this FEA modeling effort quantifies the time and effort commitment of creating a high-fidelity deployment model and highlights the limitations of the multibody dynamics modeling approach.

II.   Dynamics of Folded Deployable Structures Review

Design development of deployable structures is primarily achieved through iterative prototyping and testing: a process that often yields novel research products that are shared through the community. Specifically for deployment dynamics, validation and verification are primarily achieved through rigorous testing; and this is sometimes presented in tandem with complex finite element simulation or a simplified model approximation. A review of relevant deployment dynamics studies in the literature is presented as follows:

Deployment testing examples in the literature demonstrate several metrology methods for capturing adequate data of the deployment. The simplest validation that is often provided is a visual demonstration, either through video or sequential photography, of the deployment. This method has been published for the Ka-Band Parabolic Deployable Antenna (KaPDA) antenna [18], the Multi-Arm Radial Composite (MARCO) parabolic antenna [19], as well as many other structure concepts. This method is considered sufficient for controlled deployments, as were the KaPDA and MARCO antennas, but can be questionable for a free-deploying system where the dynamics are not controlled and are less predictable (and potentially less repeatable). A useful videogrammetry system for deployment dynamics testing is provided by motion capture systems. This system directly measures the position of multiple reflective targets on a moving body of interest through time. A notable test campaign that implements this in the literature features the Self-contained Meter-class deployable boom (SIMPLE) meter-class boom [20], which demonstrated a free deployment of a self-actuated boom.

Considering now the modeling portion of the literature, there are few studies that developed modeling techniques for free-deploying strain-actuated spacecraft structures. One significant study of the free-deployment dynamics of a tape spring actuated system was provided by the Mars Advanced Radar for Subsurface and Ionosphere Sounding (MARSIS) antenna project that flew on the ESA's Mars Express and was deployed in 2005 [21]. This antenna comprised three z-folded tubes, the longest of which was 40 m and had 12 folding hinges. A significant anomaly occurred during the deployment of the first boom, where a tape spring hinge did not deploy, and therefore created an intermediate deployment shape. Additional modeling efforts were needed to determine the partially deployed state, to determine the cause of the anomaly, and to design a spacecraft maneuver to correct it [22]. In these studies, a multibody dynamics modeling software (Adams) was implemented to model the deployment, treating the tape springs as spline hinge joints. Additionally, Abaqus finite element simulations were created to validate the Adams model at the component level, modeling only a single hinge connecting two tubes, due to the infeasible computational cost of modeling a full system. Major takeaways from this study are the risks taken in not being able to do a ground deployment test and the importance of predicting hinge behavior. An additional study of Adams demonstrated the software's capabilities in modeling difficult benchmark problems [23] and discussed the limitations. Including higher-fidelity effects, such as contact and bending, is not an objective of the multibody dynamics model implemented here, and therefore Adams was not considered for this study.

An additional example is a self-actuated z-folded solar array for CubeSats that included a finite element model and a deployment test using Vicon videogrammetry [24]. This system consisted of several 10-by-10 cm panels connected by flexure hinges at the folds. This study found issues with the panels self-contacting through deployment, where the likelihood of such behavior for systems of more than seven panels was high. Additionally, there was large variance in the deployment path of the array, although there was good correlation for the

deployment time and final deployed distance between the simulations and experiments. Although these two studies provide clear approaches to studying free-deploying systems, they are both z-folded open-chain systems not subject to closure constraints, which is the dominant challenge of an origami structure. A study of the deployment of a self-deployable origami-folded structure has been seen in the literature [25]. The authors created a deployment dynamics model using commercial modeling software that includes linear stiffness models of strain joints with multiple degrees of freedom. However, this system included a cable system, and deployment dynamics of the design were not tested or correlated in the study. Additionally, strain joints and tape spring hinges have notable differences in behavior properties.

The last idea to consider is representing hinge behavior with a reduced model. A similar concept of representing a complex mechanical hinge with a force/torque model for dynamics modeling has been demonstrated using an integrated finite element and multibody software [26] for a folded open-chain solar panel deployment. These hinges were traditional mechanical pin and clevis (or piano) hinges, where unlike tape spring hinges, the internal contact was the behavior of interest. This study demonstrates interest in the community in developing reduced hinge modeling techniques to better understand deployment dynamics simulations.

This review highlights the current progress in the deployable space structures community on the topic of deployment dynamics analysis for structures with folding hinges. The research presented in this paper then sits at the intersection of several state-of-the-art elements, namely, the modeling of high strain elastic hinges, dynamics modeling for origami-folded structures, and the design and implementation of free-deployment strategies for origami-inspired space structures.

III. Folding Structure Prototype and Deployment Testing

The objective here is to design and build a folding structure that can be used to qualitatively evaluate the dynamics modeling approach. A prototype structure is developed, and a deployment testing campaign is conducted. A concept illustration of the deployment test system is displayed in Fig. 2, where a four-body structure is shown suspended by gravity offload lines and a gravity compensation system of countermasses. The deployment tests include two sets of trials: one in the "cup-down" configuration, where the folded structure creates a "cup" that faces the ground during deployment; and a "cup-up" orientation, where this cup is facing the ceiling. These two sets of data can be used to observe any residual influence of gravity remaining beyond what is offset by the gravity compensation system.

A. Four-Body Prototype Design and Build

The prototype is developed for the simplest closed-chain system case: the four-body structure case. The panel pattern is modeled after the base unit of the Miura-ori pattern, where the fold line geometry of the theoretical pattern is designed such that there is only 1 deg of freedom through folding and unfolding. This makes the pattern ideal for space structures applications. Two tape spring hinges are implemented across a single fold line of the pattern, where spring steel tape spring hinges are used in the prototype build and are modeled in Sec. IV. The prototype structure is shown in the deployed configuration in Fig. 3, where several features are shown. A 60 deg Miura fold angle is chosen for the fold panels to maximize the stability of the folds, resulting in each panel having a parallelogram shape. The edges of the panels are each 337.3 mm long and chamfered to reduce the influence of contact dynamics in the
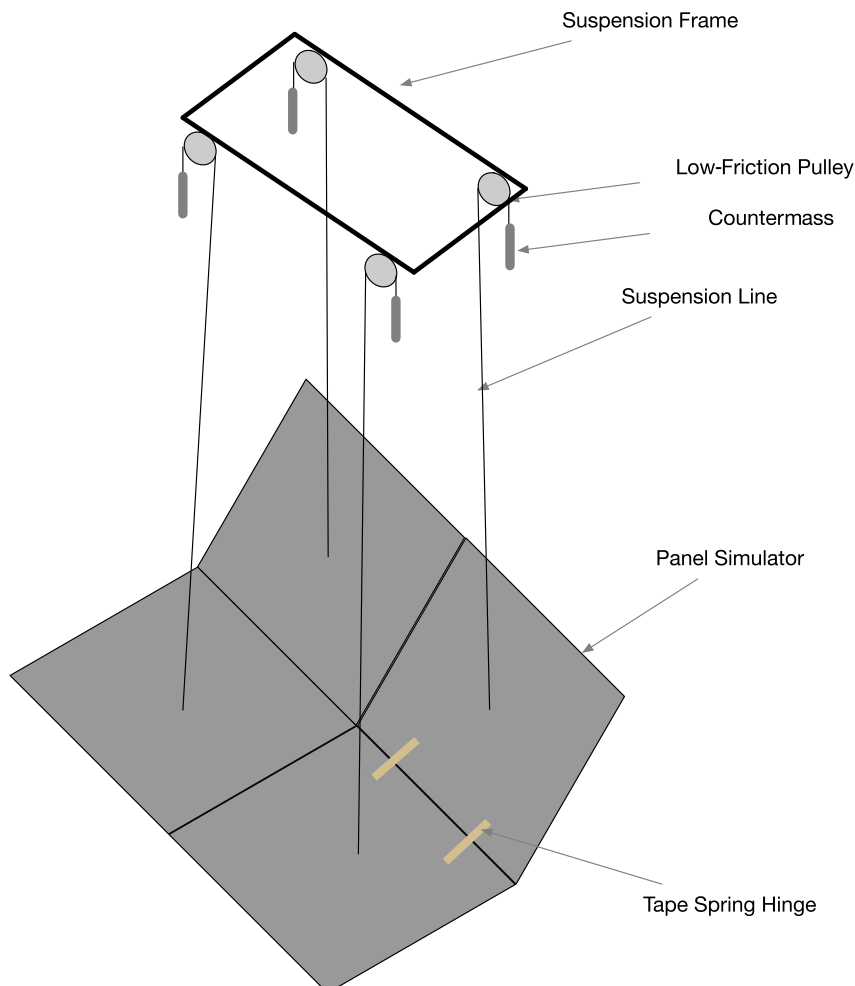

Fig. 2 Concept illustration of the gravity offloading system and structure prototype (not to scale).
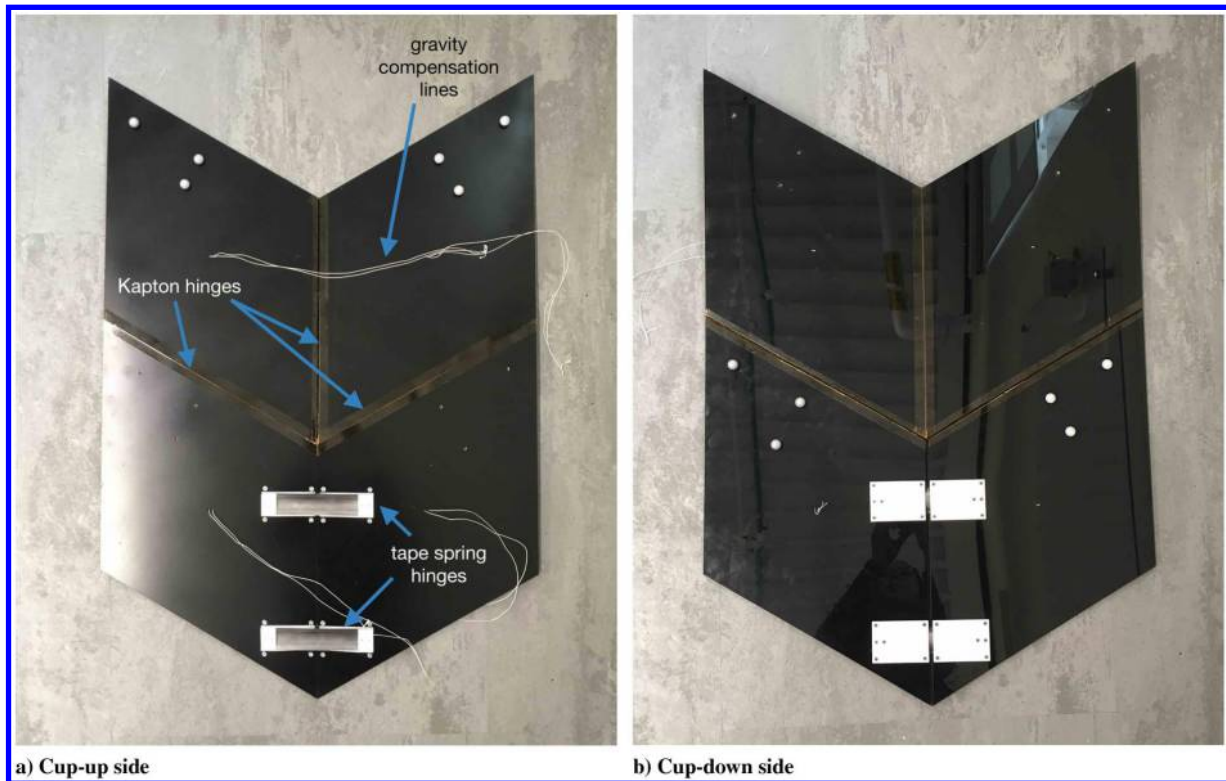
a) Cup-up side   b) Cup-down side

Fig. 3 Prototype structure in fully deployed configuration.

deployment. These edges are attached using thin, 0.0025 in. Kapton tape such that the fold axis of the edge is approximated as the physical edge of the panels. Because thicker material is used for these fold lines, the influence of the material as it curves may become a concern. The tape spring hinges are observed on the lowest panels, where the mounting fixtures are manufactured from three-dimensionally (3-D) printed polylactic acid (PLA). Additional physical properties are listed in Table 1.

The physical separation of the two panels along the fold line is a novel advantage for an origami-inspired structure. This opens the possibility of a flat-folded origami pattern, where the thickness of the panels would require extensive design of the fold line placements to ensure flat foldability [27,28]. Using segmentation to enable physical implementation of an origami-inspired pattern due to material thickness is demonstrated by the novel slipping fold design presented by Arya et al. [29] for membrane structure applications. Another example of adapting origami for thick folding was presented by Hernandez et al. [30]; however, their application did not include tight packaging for spacecraft purposes. The hinge design presented here offers another approach to this challenge as applied to rigid or semirigid folded structures, and a basic diagram of this concept is shown in Fig. 4. Figure 5 displays the prototype structure in a nearly folded configuration and suspended in the cup-down orientation. From the hinge view, the multiple degree-of-freedom (DOF) status of the tape spring hinge edge is revealed, where the edges have translated apart and the panels are rotated slightly open, in addition to the primary fold rotation. The panels are able to separate completely, and their relative position and orientation demonstrate multiple-DOF offsets.
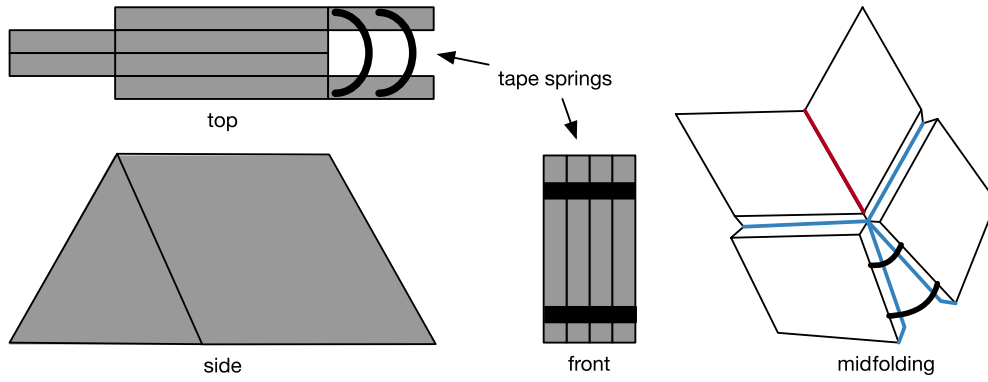
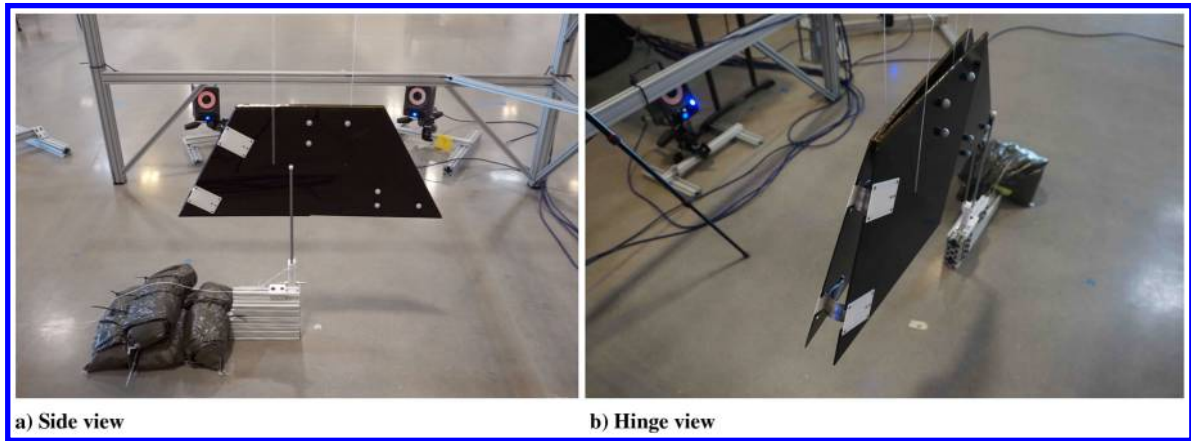### B. Four-Body Prototype Deployment Test Bed

Deployment testing of the prototype must provide gravity compensation, measure each panel body's positions in 3-D space through the deployment duration, and operate at sufficient resolution through the deployment duration. These requirements are met by developing two systems: a suspension system that provides gravity offloading, and a metrology system that is capable of taking the desired measurements.

The approach for gravity compensation for the deployment testing is designed as follows: Each panel of the system is treated as a rigid body. The attachment points of the gravity compensation lines are placed at the center of mass of each rigid body using a line tie point. The center of mass of each flat panel is determined from the panel geometry using CAD mass property evaluation tools. The placement of these points determines that the deployment must be tested in either the cup-up or cup-down configurations. A concept diagram of a gravity offloading system and four-body prototype is shown in Fig. 2. The mass of each panel is compensated for using a countermass made from narrow bottles of lead shot. The countermasses are calibrated carefully by hand such that a small angular or linear velocity perturbation along any axis of the structure is not restored by the compensation system, and the velocity is not damped over acceptably small motion ranges. This ensures that the gravity compensation system is not significantly influencing the dynamic response of the deployment. Each gravity compensation line is made from braided spectra and is approximately 6 ft long, where the length is limited by the offload frame. The braided spectra line is selected to eliminate dynamic flexing from the lines. The influence of the static offload point on the deployment is considered negligible, where the translation difference is an order of magnitude smaller than the suspension length. Finally, a detached clamp system is designed to hold the structure in the folded state at the initialization of the test, and it is displayed in Fig. 5. This clamp is activated using a pull pin to release and a stiff torsion spring to quickly open the clamp and move the clamp arms out of range of the structure as it deploys.

The metrology system selected for this testing implements the Vicon MX T-series cameras and Tracker 3 software by Vicon Motion Systems. This is a motion capture system that is designed to track discrete targets in three-dimensional space and has established applications for deployable structures testing [20]. Ten Vicon cameras are installed

Table 1 Properties of the prototype parts

Part	Material	Mass, g	Thickness, mm	Length, mm
Panel	Cast acrylic	350–369	3.2	292 along edge
Hinge plate	PLA	7.8	NA	N/A[a]
Tape spring	Spring steel	4.6	0.15	150

[a]N/A denotes "not applicable."

Fig. 4 Three-view illustration of a thick flat-folded Miura pattern unit with tape spring hinges embedded. A midfold view is also included, where red indicates a valley fold and blue indicates a mountain fold.

Fig. 5 Prototype structure in folded configuration in test bed.

Fig. 6 Reference frames defined in Vicon denoted as $\mathcal{P}$, and hinge frames denoted by $\mathcal{H}$. Body reference numbers are also included.

position in the camera frame of less than 60 μm. High-precision spherical targets of 14 mm in diameter are installed on the prototype and are visible in Fig. 3; and they are tracked to provide position and orientation data on each of the four panels. Figure 6 displays the panel and hinge frames defined from the spherical targets. Data are collected at a frame rate of 100 frames per second, providing sufficient resolution to observe the dynamic response well. A selection of camera frames from the deployment is shown in Fig. 7 to illustrate the deployment behavior of a single trial. Test results and experimental data are displayed and discussed in Sec. V. Two trial sets of 15 trials were completed: one set in each of the cup-up and cup-down orientations to consider two orientations relative to gravity so that a qualitative assessment of the gravity compensation can be made. All datasets have been treated with a five-point moving average smoothing algorithm on the raw measurements to reduce the appearance of noise. The initial conditions of each trial are found to not be absolutely the same for each case, due to the limitations of the fold clamp and the flexibility of the tape spring hinges. Generally, the cup-up trials have a slightly deployed initial angle of 177 deg, versus the more closed 179 deg of the cup-down cases. This difference in initial conditions is shown to be the primary influence in discrepancies between the two trial sets, and not the influence of gravity. The cup-down trials consistently deploy faster than the cup-up trials because there is more strain energy in the cup-down initial conditions. Both cup-up and cup-down initial conditions are therefore considered when comparing to the multibody dynamics modeling.

around the gravity offload frame. These cameras are calibrated using a precision calibration tool that enables the Tracker 3 software to learn the camera's position in space. The results of the calibration used in the test trials state that each camera has an error in knowledge of a target's

IV. Steel Tape Springs Hinge Models

Spring steel tape springs are selected for the folded deployable structure study because the behavior of this material is well known and the simulation of the behavior in a finite element software is more reliable. A force-displacement and moment-rotation model of
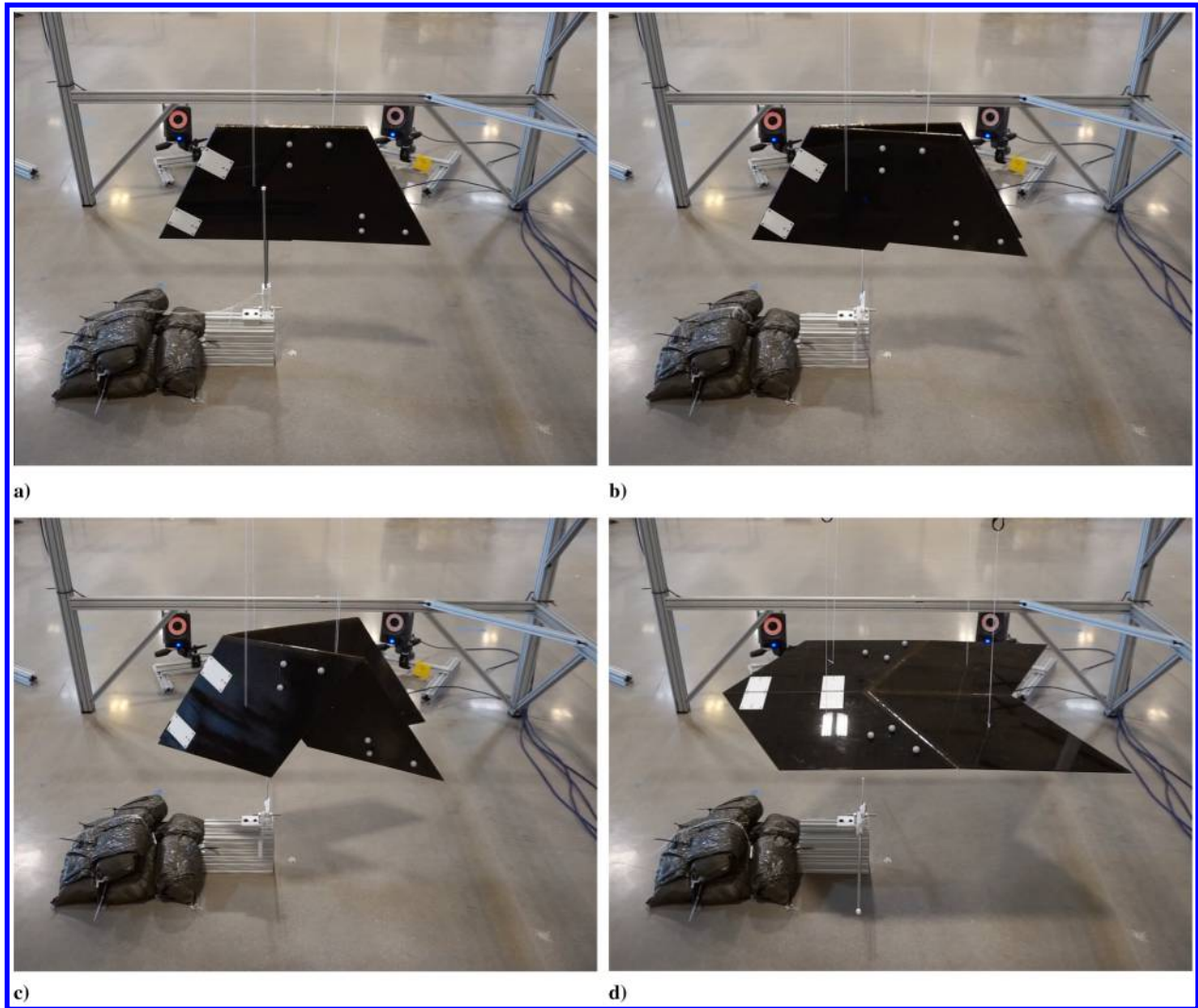
Fig. 7   Prototype structure through deployment sequence. A video is available in the Supplemental Material.

the tape springs is needed to represent the hinge in the multibody dynamics simulations. Data for this are generated from a finite element model for this study and are considered sufficient due to the well-established properties of the hinge materials, and therefore a hinge experiment is not conducted for the spring steel tape springs. A study of developing this approach for high strain composite hinge modeling, including experimental analysis, demonstrated performance with special consideration for the complex composite material [16]. This section provides the details of the hinge relative state model definition, data library generation, the nonlinear regression models, and a statistical evaluation of the model fits.

Several research studies characterize the moment-curvature behavior of tape spring hinges for various materials by assuming the hinge folds symmetrically, meaning through only one rotational degree of freedom. Typically, the equal-sense and opposite-sense bending moments are characterized through theoretical analysis and experimental testing, as well as empirical modeling [31,32]. Here, equal sense refers to a fold where the open cross sections face each other, and opposite sense is a fold where the open cross sections face away, as is consistent with the tape spring literature (and can be viewed in Fig. 8). There has been further interest in characterizing the behavior of a diagonally folded hinge [33]. These studies provide fundamental understanding of a hinge's structural mechanics behavior, focusing on failure and stiffness, as well as demonstrate their correlation with mechanics theory. However, here, the objective is to reframe the hinge as a dynamic actuator and capture the deployment behavior of a system as actuated by the hinge. The tape spring introduces unique challenges from this perspective. A typical fold

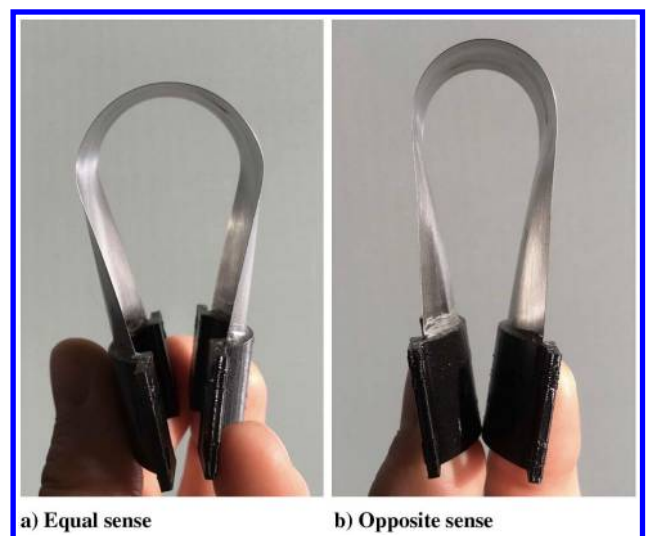

Fig. 8   Fold orientations of a high strain tape spring hinge.

joint is treated as a single-DOF revolute joint where the attachment points on each connected body are coincident and have one relative rotation. Under certain assumptions, the symmetric behavior of the tape spring hinge can be modeled as a single rotation where the moment-curvature behavior describes the internal torque due

to the hinge. However, the connection points are separated by the length of the hinge and will be displaced from each other over the deployment. The actual force and torque response of the hinge will depend on the loading of either side of the hinge, and small displacements from the nominal configuration may introduce significant force and torque responses. Therefore, the established moment-curvature approach is not sufficient for the modeling fidelity desired here; and a study of force and torque responses due to nonsymmetric behavior is conducted.

The phenomenon of undesirable nonsymmetric configurations in the tape spring hinge fold is not well studied. Here, nonsymmetric behavior refers to any change in position and orientation that does not follow the nominal fold rotation, as is illustrated in Fig. 9. To guarantee symmetric behavior, additional components must be included in a hinge assembly to constrain the hinge, which can add mass and complexity where lightweight simplicity is desired. Such solutions are not addressed here. Inclusion of multiple independent state variables in this study makes it difficult to approach the problem with classical theory; therefore, to study this phenomenon, numerical techniques are employed to create an empirical model of hinge behavior.

A. Rigid-Body Dynamics and the Six-State Hinge Model of Forces and Torques

The tape spring hinge is represented in the rigid-body dynamics simulations as an internal forcing function in terms of the position and orientation of the hinge connection points. This concept is illustrated in Fig. 9, where the fixed end points of the hinge are each assigned a reference frame ($\mathcal{A}_0$ and $\mathcal{A}_1$), the reaction forces from the hinge are denoted as N_0 and N_1, and the reaction moments are denoted as M_0 and M_1. These mechanics are modeled as functions of the relative position δ and orientation of frame $\mathcal{A}_0$ with respect to $\mathcal{A}_1$.

The hinge model is developed to be compatible with a preexisting multibody dynamics framework based on the spatial operator algebra multibody dynamics approach [34]. This approach deconstructs a system of linked rigid bodies by defining the interactions across the hinge connecting an outbound body to an inboard body through relative coordinates and selecting these as the generalized coordinates of the dynamics model. The framework of the algorithm then calculates the system dynamics having only needed the relative hinge definitions and rigid-body properties. To provide consistency with this, the generalized coordinates are selected to be the displacement of the relative hinge frame coordinates and the relative orientation:

$$q = \begin{bmatrix} \theta(\mathcal{A}_0, \mathcal{A}_1) \\ \delta(\mathcal{A}_0, \mathcal{A}_1) \end{bmatrix} \quad (1)$$

For this analysis, all dynamics quantities are expressed with respect to the hinge origin frame defined as the inbound frame $\mathcal{A}_0$. This lends insight into how the hinge affects any inbound body directly, as well as how an outbound body is affected relative to the inbound body. This information can be easily transformed to desired frames as needed. The hinge origin frame is oriented on the hinge such that the third axis a_{0_3} pointed down the length of the hinge a_{0_2} is normal to the hinge cross section, and a_{0_1} completes the right-hand
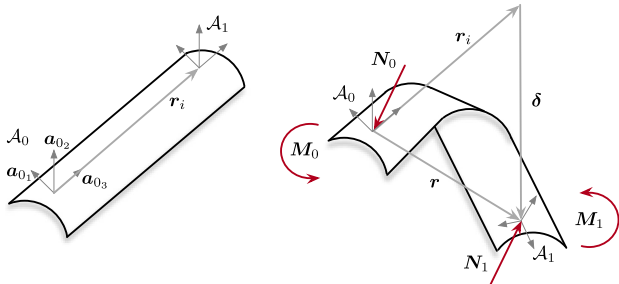
convention. The relative orientation $\theta(\mathcal{A}_0, \mathcal{A}_1)$ contains 123 Euler angles for ease of interpretation and because the second axis, where the 90 deg Euler angle singularity resides, can be oriented with an axis that does not accommodate significant relative deflection. The $\mathcal{A}_1$ frame is oriented identically to the $\mathcal{A}_0$ frame when the hinge is deployed in the zero energy state. The displacement of the relative hinge frame coordinates δ is selected over the relative position r to better correlate the physical behavior with the numerical fit. The relation of these vectors is displayed in Fig. 9, which is defined as

$$\delta = r - r_i \quad (2)$$

Then. the generalized forces and torques acting at frame $\mathcal{A}_0$ are written as a function of the relative coordinates across the hinge frames, in spatial notation, as

$$f_0(q) = \begin{bmatrix} M_0 \\ N_0 \end{bmatrix} = \begin{bmatrix} M_{0_1} & M_{0_2} & M_{0_3} & N_{0_1} & N_{0_2} & N_{0_3} \end{bmatrix}^T \quad (3)$$

B. Model Estimation and Nonlinear Regression Approach

The next objective is to determine adequate empirical models for the six entries of $f_0(q)$. There are several options for determining response functions that include large multivariable datasets. Simple approaches include using a lookup table or interpolation between data points. However, these will not necessarily provide insight into predictor variable relationships and cannot be further manipulated. Therefore, a function fit is desired. A polynomial containing both first-order and second-order coupled polynomials is first proposed for capturing the nonsymmetric relationships, where the number of coefficients would be excessive for higher-order polynomials:

$$p(q) = \sum_{i=1}^{6} a_i q_i + \sum_{j=1}^{6} \sum_{k=1}^{6} b_{j,k} q_j q_k \quad (4)$$

For the symmetric fold, it is suggested from the literature that the nominal fold produces a pure moment in the symmetric case, and this moment can be represented empirically using a seventh-order polynomial [31]. However, in this study, the best-fit empirical regression model is determined to be a piecewise nonlinear function of the form

$$M_{0_1} = \begin{cases} \sum_{i=2}^{6} a_i \theta_1^i + \sum_{i=1}^{4} b_i \frac{1}{(\theta_1 + \epsilon)^i} & \theta_1 > 0 \\ c_1 \theta_1 + c_2 \theta_1^2 & \theta_1 < 0 \end{cases} \quad (5)$$

where the inclusion of the inverse polynomial terms in Eq. (5) greatly increases the fitting performance for the theoretical peak moment due to snapthrough of a tape spring hinge, as seen in Fig. 10. In this expression, θ_1 is the Euler angle about axis 1 (or the nominal fold angle on the primary hinge axis); $\epsilon, = 0.001$ is a small numerical buffer to prevent numerical issues at zero; and a_i, b_i, and c_i are the coefficients to be determined through regression techniques. A nonlinear regression approach is best suited for the nonlinear, multivariate model functions in Eqs. (4) and (5). For practical applications, a unique regression should be fit for tape springs of different materials or geometry. The Statistics and Machine Learning Toolbox published for MATLAB is used to fit and evaluate the models. The quality of the fit is evaluated by several means. The toolbox is further used to acquire an R-squared estimate, the root-mean-squared error (RMSE), and the histograms of the raw residuals. The coefficient of determination (R squared) is meant to indicate how much of the variation in the response is captured by the model and is expressed on a scale of zero to one, where the fit is better the closer it is to one. For a nonlinear regression, the R-squared value is not entirely trustworthy but is included here for initial evaluations. The root-mean-squared error is the average standard deviation of the fit, and the residual histograms provide a full picture of how variable the fit is.
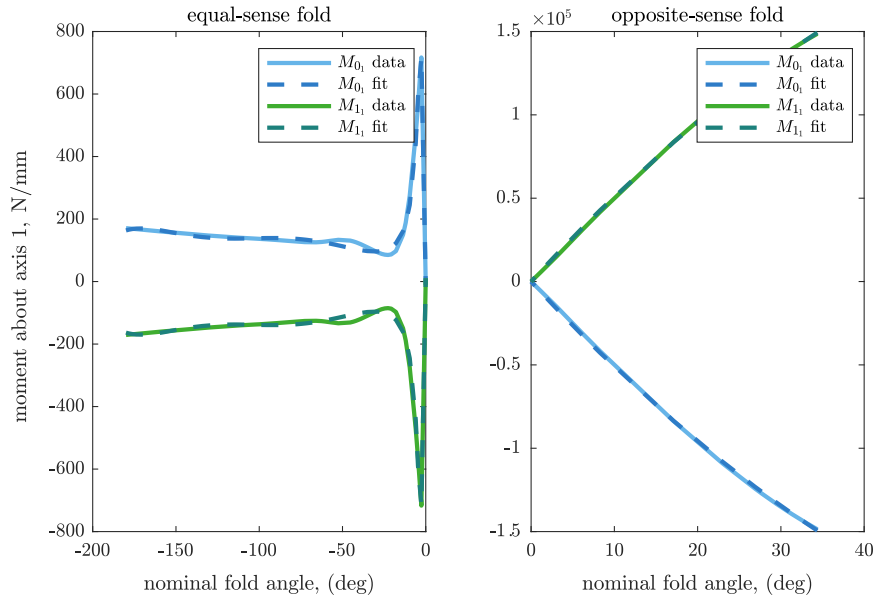

Fig. 9 Definitions for a tape spring hinge in deployed (left) and nonsymmetric (right) configurations.

Fig. 10   Nonlinear regression fit curves for the nominal fold hinge data.
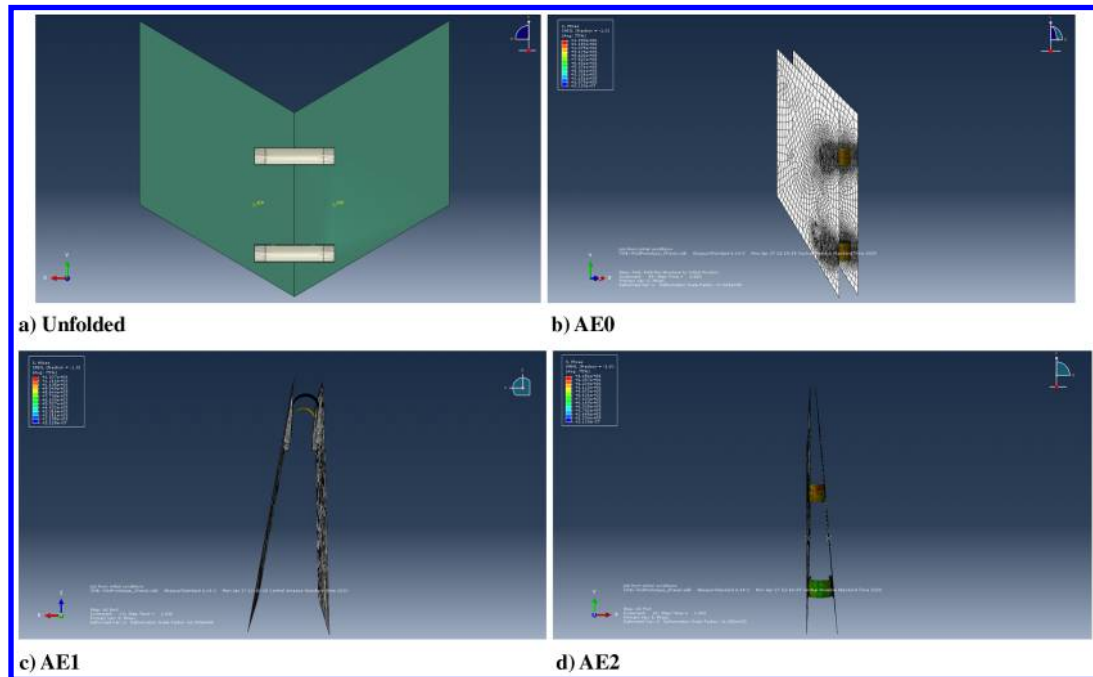

Fig. 11   Implementation of two tape spring hinges on a single fold line of two panels and examples of displacements implemented in Abaqus where the symmetric angle is ±90 deg.

C.   Prototype Tape Spring Actuated Hinge Design

The folded deployable structure prototype hinge design is as follows. For this study, only the fold line where tape spring hinges are embedded is of immediate interest. Two tape springs are embedded to

Table 2   Hinge geometry for spring steel tape springs as measured and implemented in the FEA models

Parameter	Value
Material	Spring steel
Elastic modulus, GPa	200
X-section radius, mm	22.46
Arc length, mm	29.21
Thickness, mm	0.15
Length, mm	150

provide stability, to reduce the degrees of freedom, and to provide sufficient torque for deployment. This configuration of this hinge design is displayed in Fig. 11, as depicted in the Abaqus 6.14 user interface. The tape springs are identical, and their relevant geometry and material properties are reported in Table 2. One hinge model is created from the two-tape-spring configuration shown in Fig. 11, to be used in the multibody dynamics model. The multibody dynamics model defines the relationship between two bodies and is not sophisticated enough to implement two relationships for the same two bodies.

D.   FEA Hinge Model Construction

The finite element analysis simulations of hinge behavior are built in Abaqus 6.14 using a static, general analysis. The hinge is represented as a shell with elastic behavior defined by the elastic modulus and a Poisson's ratio of 0.3. The hinge mounting plates and panel assembly are represented as a discrete rigid part, and the tape springs are

constrained to them using tie constraints. The rigid panel assembly is only included to enforce the hinge boundary conditions and does not affect the hinge model generated in the static analysis. Four-node shell (S4R) elements are meshed on the hinge shell using a 2 mm mesh because this is the largest mesh size that results in successful folding of the prototype due to the large deformation of the fold radius on the tape springs, where element deformations above 20 deg are not desirable. Further mesh refinement to 1 mm or smaller mesh sizes was completed and had comparable results to the 2 mm mesh; however, a more coarse mesh was not as accurate. The largest accurate mesh is selected to reduce run time. The asymmetric configurations are implemented as displacement and rotation boundary conditions in static/general steps. Each range of asymmetric configurations is explored as a separate step enforced on an initially symmetric configuration. An asymmetric data-set is generated for each primary fold angle θ_1 at increments of 5 deg from 100 to 180 deg of the fold, resulting in nine equal-sense datasets. Asymmetries on smaller fold angles are excluded because they are unlikely and introduce Abaqus convergence issues. Figure 11 shows example profiles for the equal-sense cases with nonsymmetric displacements, with a no-added-deformation scaling.

The configuration of the hinge within the prototype design informs the definition of the asymmetric configurations. From inspection, three degrees of freedom from the six-state hinge model defined in Sec. IV.A can be excluded for this study. This is due to the fact that the prototype has single-degree-of-freedom hinges on the other fold lines,

constraining linear motion in the first and second axes and rotations about the second axis. Therefore, the configuration constraints in the model simulation contain three asymmetric configurations beyond the nominal fold. These are defined in Table 3, where the first asymmetry is on the primary degree of freedom, and the second asymmetry captures the remaining observed degrees of freedom on the fold line. Considering the opposite-sense behavior of this hinge, all potential asymmetries are eliminated due to the constraining design of the panels when folded in this direction. Therefore, only the nominal fold data in the opposite sense are needed from the simulation.
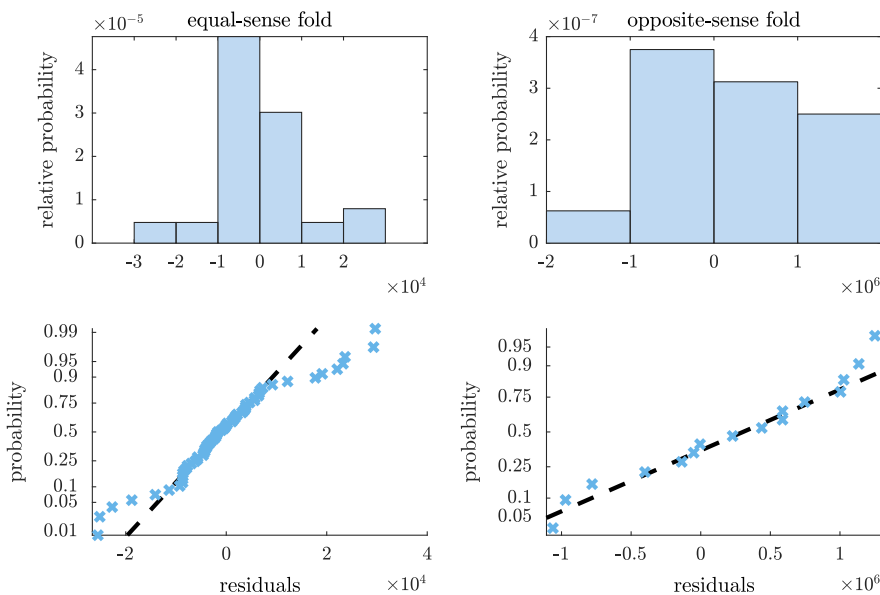
The effects of hysteresis on the tape spring moment-curvature behavior, which are dependent on the trajectory of the folding, are not included in this model. This is not necessary because the deployment direction behavior is the primary driver of the deployment, and computational and numerical issues that are observed around the asymptotic peak outweigh any subtle difference due to hysteresis.

E. Nonlinear Regression Models

The hinge profile data are fit to polynomial expressions using the nonlinear regression techniques from Sec. IV.B. Two models are created for use in the prototype deployment model. The first model is for the nominal fold torque and is only a function of the nominal fold angle. This provides an idealized model for initial evaluation of the deployment characteristics. The second model considers the full spatial force and torque profile from the asymmetric profiles of the prototype hinge. For both models, a piecewise function is designed for the primary moment such that the equal-sense and opposite-sense behaviors are modeled independently. This provides a much more accurate behavior model, where the opposite-sense fold behavior is significantly different due to the presence of the rigid-body panels and restricted freedoms due to contact with the panels.

1. Nominal Fold Moment

The resulting coefficients are reported in the Appendix in Table A1, and the fit function is plotted over the source data in Fig. 10. Additionally, the statistic evaluations of these regressions are reported in Table 4; and the histograms and normal probability are shown in Fig. 12, where the residuals of the fit are shown in blue and indicate the fit is centered around zero, confirming the quality of the fit. The RMSE for the opposite-sense case is much higher due to the stiffness of the system folding in the opposite-sense direction. For this same reason, the opposite-sense fold angle range is limited because the structure will not be able to fold very far in this direction. The nonlinear regression model for the nominal fold data is seen to be a strong fit in both the

Table 3 Asymmetric boundary conditions used to generate Abaqus (A) datasets in both equal (E) and opposite (O) folds of the prototype structure hinge, defined in an inertially fixed frame

Case	θ_1 symmetric, deg	θ_1 offset, deg	θ_2, deg	θ_3, deg	δ_1, mm	δ_2, mm	δ_3, mm
AE0	0–180	0	0	0	0	0	Free
AE1	100–180	±10	0	0	0	0	Free
AE2	100–180	0	5	0	Free	Free	Free
AO0	0–30	0	0	0	0	0	Free

Table 4 Nonlinear regression fit statistics for the nominal fold of the prototype hinge

Statistic	Equal sense	Opposite sense
R squared	0.99	1
RMSE, N/mm	11.3	814

Fig. 12 Fit function histogram and normal probability for the nominal fold simulation data.

Table 5   Statistics for the fit functions of the
prototype hinge assembly model

Statistic	M_{0_1}	M_{0_2}	M_{0_3}	N_{0_1}	N_{0_2}	N_{0_3}
R squared	0.96	1	1	0.99	0.87	0.93
RMSE	14.3	5.6	4.5	0.005	0.01	0.02

equal- and opposite-sense cases. The model histograms show a near-Gaussian distribution with no outliers, and the normal probability is approximately linear as expected. This model therefore provides a sufficient representation of the hinge behavior when restricted to a single-degree-of-freedom deployment demonstration.

2. Six-DOF Asymmetric Fold Moment

The proposed polynomial from Eq. (4) is implemented for the secondary forces and torques of the steel tape springs prototype hinge model using the asymmetric data library, and coefficients are reported in Table A2 in the Appendix. The primary moment M_{0_1} is found to be sufficiently modeled with just the expression of Eq. (5) using the steel spring hinge data library as well, and the coefficients for this case are recorded in Table A3 in the Appendix. The opposite-sense behavior of the hinge is modeled with the same data of the one-DOF model in Sec. IV.E.1. The RSME and R-squared values for each fit are shown in Table 5, and the fits are for all but the second axis force are all in a high percentile with relatively small RSMEs compared to the force and torque magnitudes. The histograms in Fig. 13 reflect this, where the fits fall in a narrow distribution with few outliers. These force and torque models are therefore sufficient for use in the demonstration of a multi-DOF hinge actuated deployment.

V.   Results: Multibody Model Deployment Dynamics Prediction

A multibody dynamics model is developed from an approach outlined in previous work [15,17] by the authors. The approach implements a spatial operator algebra framework and is based on the articulated body forward dynamics algorithm to simulate the dynamics of origami-inspired systems. The framework is customized for this application, and is therefore computationally efficient; however, challenges from constraint violation management are acknowledged. Two deployment simulations are presented with the multibody dynamics model, absent of contact or damping effects. The first simulation implements the 1-DOF hinge model in an idealized 1-DOF fold. The second simulation implements a 4-DOF hinge definition with a multi-DOF hinge force and

torque model. The idealized 1-DOF simulation shows a smooth deployment behavior with a predicted time to peak deployment at 0.70 s, as seen in Fig. 14. Additionally, the spacecraft motion is shown in Fig. 15 and the constraint violations are shown in Fig. 16. The multi-DOF models, on the other hand, show a behaviors curve that more closely tracks the experimental models and exhibits small oscillations, as well as peak deployments at 0.82 and 0.92 s for the two sets of initial conditions, as seen in Figs. 17 and 18. Again, the spacecraft motion is shown for this case in Fig. 19 and the constraint violations are shown in Fig. 20. Both models exhibit unstable constraint violations at peak panel deployment that can be attributed to the asymptotic behavior of the hinge model around this state, where deployment is driven entirely by hinge strain energy. This identifies a central challenge for modeling the deployment dynamics of free-deploying structures with a fast deployment. The computation time for the 1-DOF model is 6.7 s; and for the 4-DOF model, it is 6.3 s to simulate 1 s of deployment. The simulation is run on a machine with a 2.5 GHz quadcore Intel Core i7 processor with 16 GB of memory, using a fixed-step fourth-order Runge–Kutta integrator.

A.   One-DOF Hinge Deployment Model

The initial conditions for the simulation are provided in Table 6 and are selected for the idealized flat-folded relative angles. All initial rates are set to zero. The hinge between panels 4 and 3 is restricted to a single-degree-of-freedom rotation about the first axis. The simulation is shown in Fig. 14 to predict a smooth deployment behavior, with peak deployment occurring at 0.7 s. After the structure reaches a fully deployed configuration, however, the structure enters a difference folding mode, where only the folds at hinges 2-1 and 4-3 are changing; and folds 3-2 and 4-1 remain open. This can be interpreted as the structure folding in half, and it is not observed during the testing. Note that the orientation angles are expressed in the relative hinge frames defined in Fig. 6. This discrepancy is attributed to the presence of unmodeled contact in the prototype, where contact along the chamfered edges of Kapton hinges prevents this folding mode. In Fig. 15, the states of the root body with respect to inertial space show there is a significant general tumble introduced to the system in response to the deployment. The effect of the deployment to the system states in an actual implementation of this structure would rely heavily on energy damping and contact within the structure as well as energy management techniques within the spacecraft. Figure 16 reveals a significant constraint violation at the peak deployment and indicates that better constraint management techniques are needed for accurate prediction of deployment behavior as the system crosses this state. The constraint equation requires the bodies of the system to create a closed-chain origami pattern. A perfectly constrained model would produce a zero curve for the constraint
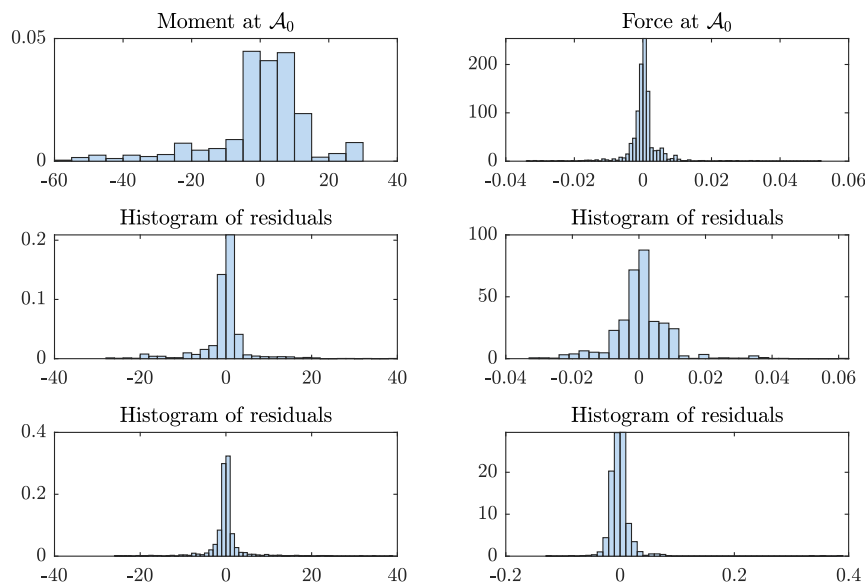
Fig. 13   Fit function histograms for the asymmetric hinge fold simulation data.
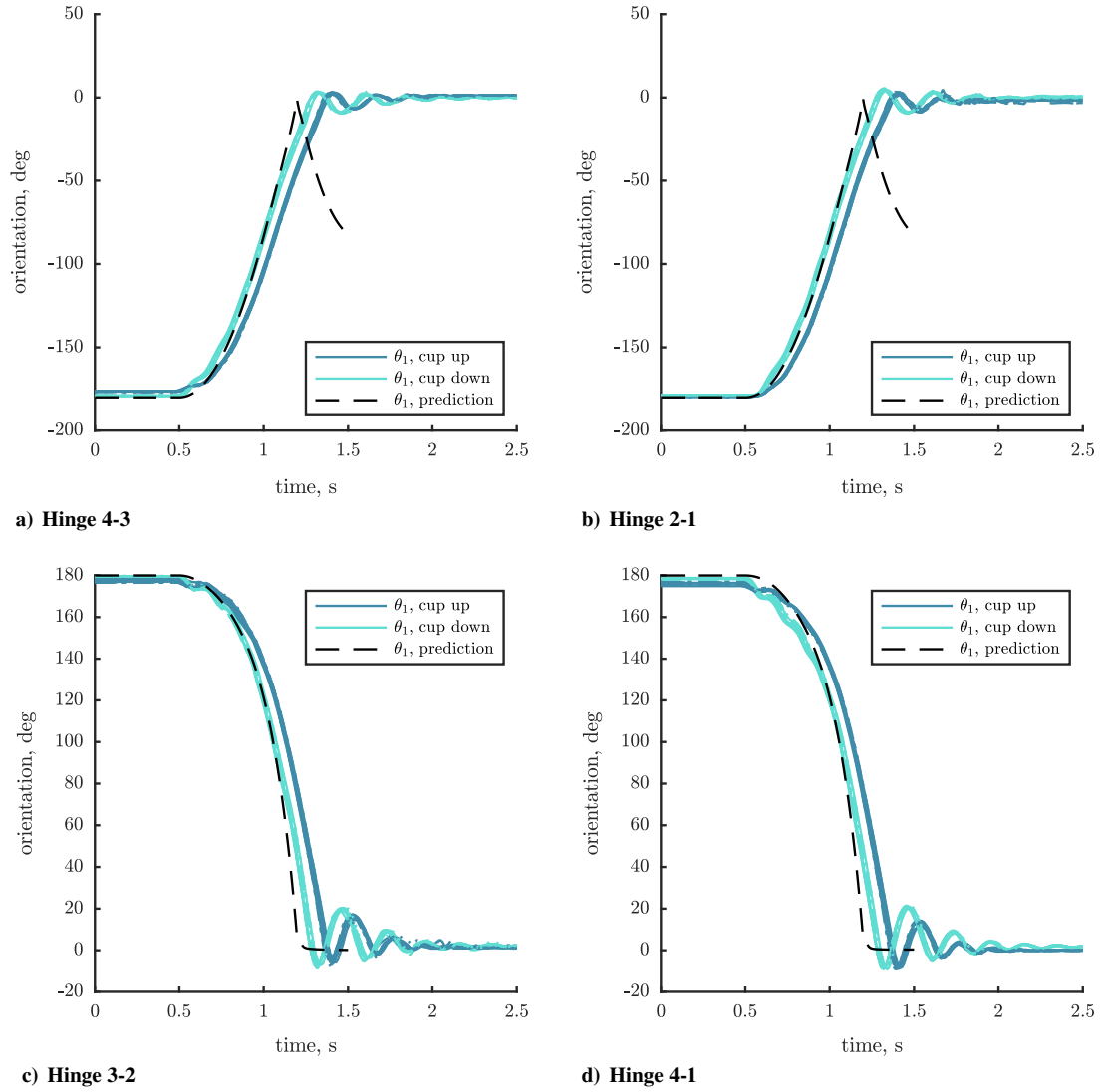
Fig. 14   Deployment actuation predictions of 1-DOF hinge simulation and experimental behavior from cup-up and cup-down trials. Orientation angles expressed in relative hinge frames defined in Fig. 6.

violation over time; and in Fig. 16, this is not the case. Constraint management such as the Baumgarte stabilization used here balances tuning the correction gains and the integration time step. This is in direct opposition to the asymptotic nature of the hinge behavior close to the deployed configuration ($\theta_1 = 0$), where smaller time steps will generate more data points along the asymptotic legs of the curve, producing a more erratic (and therefore unstable) behavior that is difficult to correct with a simple linear gain. It is possible to reduce the asymptotic peak of the hinge model, where the theoretical peak is often higher than the observed, and this might improve model stability.

B.   Four-DOF Hinge Deployment Model

The initial conditions of the two numerical simulations for the 4-DOF case, shown in Table 7, are set to emulate the nonideal, actual

Table 6   Initial conditions of the numerical simulation

Body	q
4	[0, 0, 0, 0, 0, 0]
1	180
2	180
3	−180

conditions of the average deployment from the cup-up and cup-down trials. Initial conditions of the two configurations differ due to differences in gravity orientation and boundary condition enforcements in the cup-up and cup-down trials. The nonideal initial conditions were not implemented in Sec. V.A because these initial conditions do not satisfy the constraint conditions of a 1-DOF hinged structure, and therefore were not stable. From the design of the prototype, the tape spring hinge fold line between panels 4 and 3 (hinge 4-3) is constrained due to the configuration of the other three hinges; therefore, two of the degrees of freedom can be removed such that the generalized coordinates are
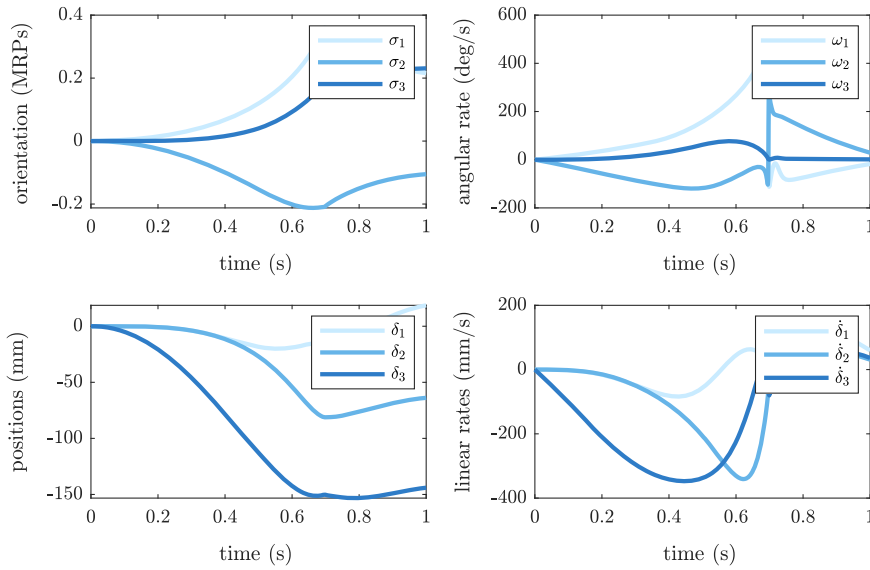
$$q = \begin{bmatrix} \theta_1 & \theta_2 & \delta_2 & \delta_3 \end{bmatrix}^T \qquad (6)$$

where δ_2 and δ_3 are measured from the panel edge as shown in Fig. 6.

From Fig. 17, the numerical simulation of these four states shows good correlation of the primary fold; however, the three asymmetric states are not well predicted. The observed oscillatory behavior has a much lower frequency and greater magnitude than what is predicted for θ_2 and δ_3, and the δ_2 simulation does not predict the oscillation observed. The difference between the model and the experimental behavior may be due to further unmodeled effects from the hinge or may be influenced by unknown perturbations from the gravity compensation system. The primary angle θ_1 is observed to better track the

Fig. 15 Angular orientation and rates of the spacecraft body in three-dimensional space. (MRPs denotes modified Rodrigues parameters.)
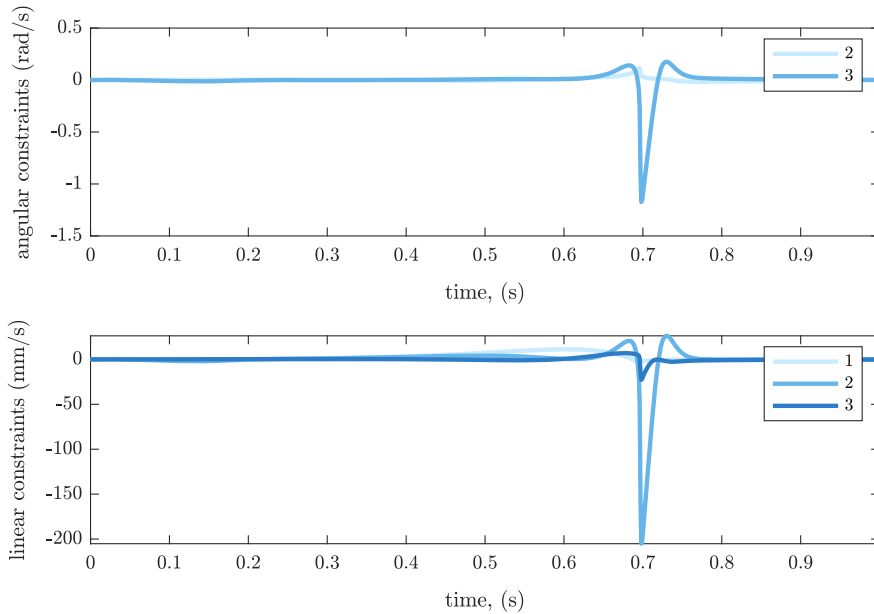
Fig. 16 Constraint violations during 1-DOF prototype numerical simulation peak as simulation enters asymptotic range of hinge behavior, where a perfectly modeled constraint would track zero.

observed behavior curve than the 1-DOF model, and the deployment peak times are closer to the observed: at 0.82 s and 0.92 s for the cup-down and cup-up initial conditions as compared to 0.83 and 0.93 s of the cup-up and cup-down trials, respectively. However, the predicted behavior at and after the snapthrough at the peak deployment is observed to quickly go unstable for these simulations. The constraint violations for the cup-up simulation in Fig. 20 show the simulation is not able to resolve the constraints near this point, and therefore the results are not reliable: particularly for the translational degrees of freedom. However, inclusion of the additional DOFs resulted in a more accurate prediction for the primary fold behavior, indicating that these DOFs have significant influence on deployment

Table 7 Initial conditions of the cup-up and cup-down numerical[a]

Body	q cup-up	q cup-down
4	[0, 0, 0, 0, 0, 0]	[0, 0, 0, 0, 0, 0]
1	176.1 deg	179.6 deg
2	177.5 deg	178.5 deg
3	[−176.4 deg, 5.4 deg, −3.5 mm, −24.6 mm]	[−179.0 deg, 1.0 deg, −3.3 mm, −12.1 mm]

[a]All initial rates are set to zero.
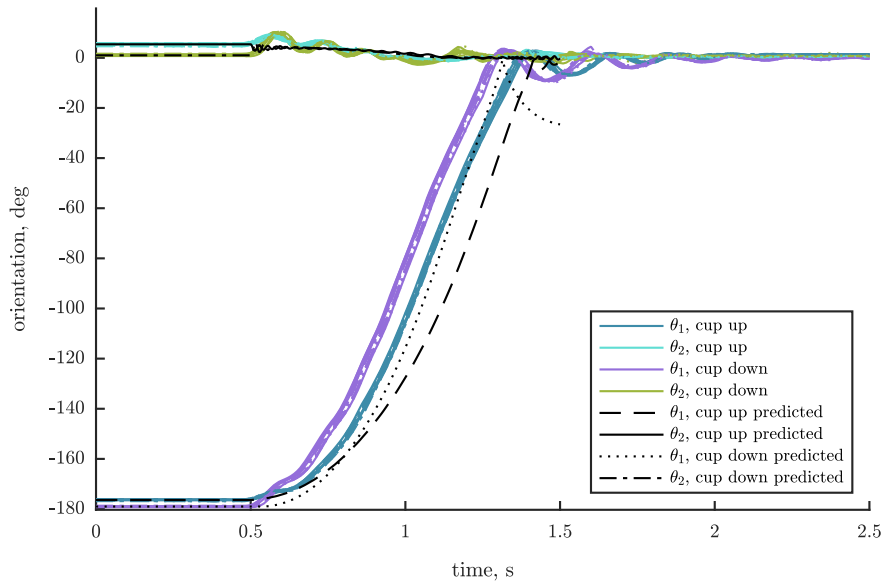
a) Hinge 4-3 orientations
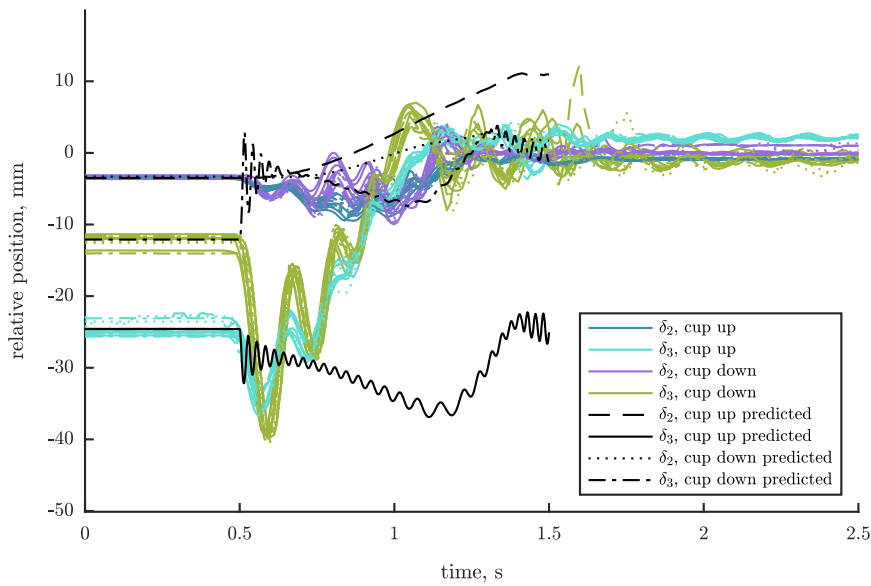
b) Hinge 4-3 positions

Fig. 17   Deployment actuation predictions of the four states of hinge 4-3 and their experimental counterparts from all trials.

behavior. Modeling challenges can partially be attributed to numerical difficulties near the deployed configuration, where there are numerical singularities when the relative orientations pass through zero, and may be having greater influence on the multi-DOF constraint equations. This behavior is also attributed to the hinge function issues highlighted in Sec. V.A, where the instability then influences multiple forcing functions across several states, and therefore yields more erratic behavior. Further investigation into the hinge model approach will yield better predictions for structure behavior, such as considering the sensitivity of the hinge model to initial conditions. The states of the other fold lines, seen in Fig. 18, show good tracking of the observed behavior for the simulations. The predicted behavior for all fold angles is seen to accelerate at a greater rate near the deployed state than what is observed, and this is attributed again to the theoretical peak moment of the tape springs. The prediction does not settle out due to a lack of contact and damping in this model. The inertial states of the root body in Fig. 19 shows very similar behavior as that in Fig. 15, predicting a general inertial tumble of the system.

VI.   Finite Element Model Comparison

A matching finite element simulation-based model provides an additional analysis that complements the research demonstrated in this paper. Although the first Abaqus model informed a hinge behavior model using static analysis, this Abaqus model will simulate the free-deployment dynamics of the prototype. A model of the prototype is constructed in Abaqus to generate deployment dynamics data and is compared to both the experimental data and the folding system multibody dynamics model. The graphic representation of this model is shown in Fig. 21 in various states of deployment. The finite element model is expected to capture more subtle behaviors in the system than the multibody model; however, the computation time is expected to reach long times. The prototype is composed of two tape spring hinges in a system subject to closure constraints in full three-dimensional space, creating additional computational complexity. This simulation provides a point of comparison for the performance of the multibody model with another approach seen in the deployable structures field for studying this kind of system. The literature lacks demonstration of FEA modeling for folding deployable structures;

a) Hinge 2-1
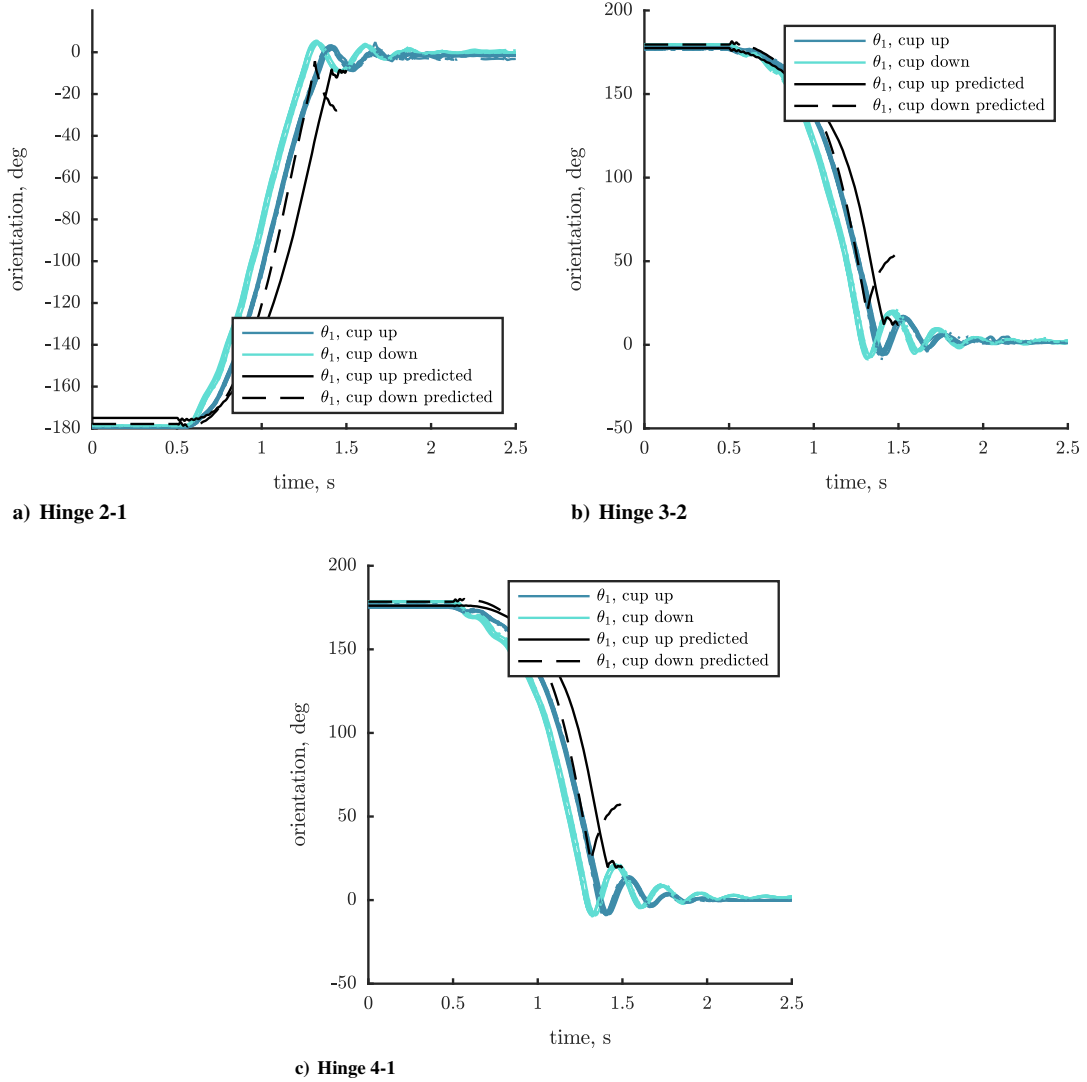
b) Hinge 3-2

c) Hinge 4-1

Fig. 18   Deployment actuation predictions of the three 1-DOF hinges and their experimental counterparts from all trials.
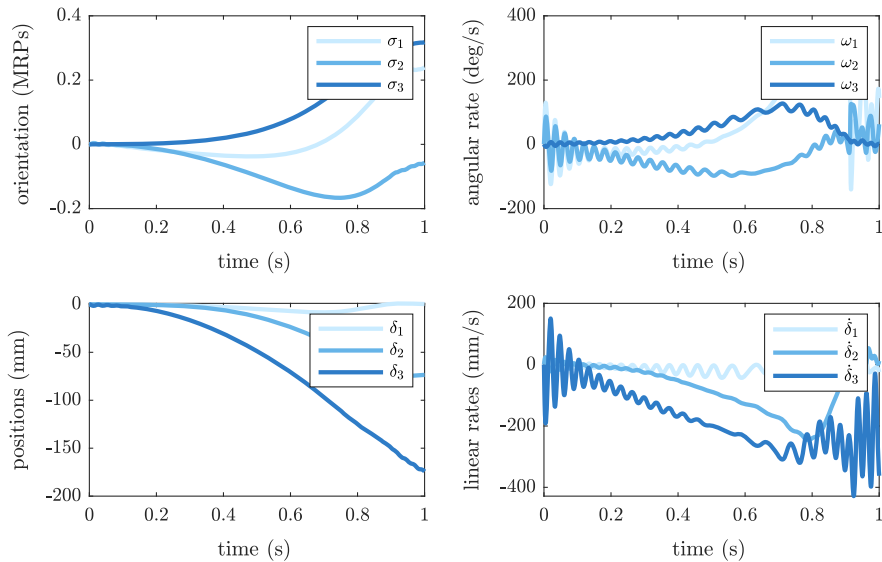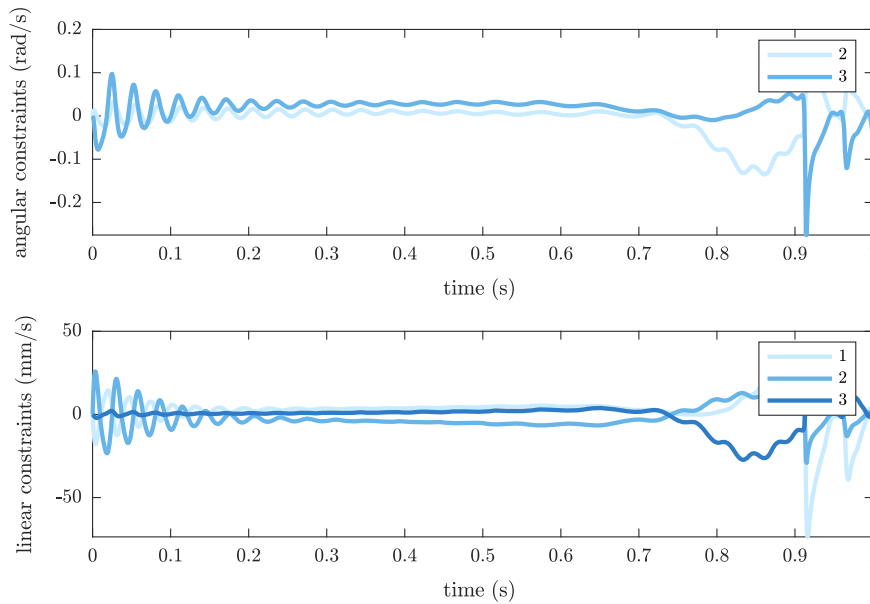

Fig. 19   States of the root body in three-dimensional space for cup-up initial conditions.

Fig. 20 Constraint violations during the 4-DOF prototype numerical simulation peak as the simulation enters the asymptotic range of the hinge behavior for cup-up initial conditions.

therefore, this study provides insights for the greater community on its relative use and performance with respect to a multibody model.

A. Abaqus Model Construction

Finite element analysis has been applied extensively to deployable spacecraft structure problems and represents the industry standard for understanding complex deformable and deployable systems. An FEA model of the prototype structure is created to provide an additional point of reference for the expected deployment behavior. FEA modeling capabilities are required in addition to multibody modeling due to the large deformation behavior of the two tape spring hinges in the system. The behavior of these tape springs as they work together in a closed-chain system is not possible to capture without the full FEA. The model is developed using the Abaqus/CAE 6.14 program. The program architecture of Abaqus heavily influences and limits the construction of the model and will now be discussed in detail. The discussion will be formatted to follow the module design of Abaqus to provide continuity for familiar users.

1. Abaqus/Standard and Abaqus/Explicit

First, the two Abaqus software packages used, Abaqus/Standard and Abaqus/Explicit, are discussed. These two packages are designed by Abaqus as two complementary analysis tools to be applied as appropriate to a wide variety of problems. Although the tools are used for similar problems, they are designed with fundamental differences in the theories applied. Abaqus/Standard provides good static analysis tools by solving for true static equilibrium in structural analysis. It also contains dynamic/implicit analysis, which is well suited for slow and stable dynamics problems. Implicit analysis uses the current information available at the current time to calculate the unknown values and requires iterations and convergence checks, which are implemented in Abaqus using the Hilber–Hughes–Taylor operator (an extension of the trapezoidal rule). Conversely, the dynamic/explicit analysis in the Abaqus/Explicit package obtains unknown values at the current time step using the information obtained from the previous time step, in what is known as an explicit dynamic integration method (or forward dynamics). Abaqus uses the forward Euler or central difference algorithm, and it adjusts the time increment to be small enough that the result lies on the curve. Abaqus/Explicit is best for dynamic problems that are high speed, have large nonlinear behavior, or are highly discontinuous. For the context of this research, the large nonlinear deformations of the tape spring hinges combined with the use of a complex system assembly requires that a dynamic/explicit analysis be used for the free-deployment simulation. Therefore, the analysis is set

up in two main phases. The first phase creates a preload condition on the system to replicate the stowed configuration of the structure, and this is completed in Abaqus/Standard. Then, the results are imported to an Abaqus/Explicit model as the initial state and a full dynamic/explicit step is run. Although it was not considered here, dynamic/explicit could have been used for the stow phase to potentially achieve a faster computation time while implementing mass scaling and damping.

2. Parts, Material Properties, and Assembly

The physical structure is represented using ten parts with the following attributes. Each panel assembly (including the Vicon targets, hinge assemblies, and hardware) is represented by a unique deformable trapezoidal shell part. This is required to minimize the complexity of the mesh and reduce the computation time of the analysis. The full panel assembly is then represented by the user input inertia properties. The properties are generated by the solid CAD model approximation, where physically measuring the inertia properties was not an option. The inertia properties are applied at the center-of-mass location of each panel for correct geometric representation. The panels are assigned elastic mechanical properties and set with the Young's modulus for cast acrylic because this is the material of the panels and additional assemblies are represented by rigid bodies. Then, four rigid-body hinge attachment plates are used to interface between the folding panels and the tape spring hinges. These parts are geometrically simplified versions of the hinge attachment plates and are modified to provide the best mesh and constraint surface definitions in the analysis. Finally, the tape springs are represented by deformable extruded shell parts with a Young's modulus for spring steel. The details of this construction are summarized in Table 8. The mesh size of the tape springs is set to 2 mm because this is the largest mesh size that results in successful folding of the prototype due to the large deformation of the fold radius on the

Table 8 Abaqus model part properties

Part	Type	Material	Modulus, GPa	Shell thickness, mm	Instances
P1	Deformable	Cast acrylic	3	3.175	1
P2	Deformable	Cast acrylic	3	3.175	1
P3	Deformable	Cast acrylic	3	3.175	1
P4	Deformable	Cast acrylic	3	3.175	1
Hinge plate	Rigid body	N/A	N/A	N/A	4
Tape spring	Deformable	Spring steel	200	0.15	2

tape springs, where element deformations above 20 deg are not desirable. Then, for successful interactions between the tape spring and the attachment plate, the same mesh size is applied to the attachment plate. The mesh of the panels is set to the recommended size of 33 mm, but it is refined to 2 mm at the region that interacts with the attachment plate: again, for interaction purposes. The sensitivity of the tape spring component to mesh size is therefore the driving factor for the mesh design. A lower-fidelity mesh would reduce computation time but would yield unreliable results.

3. Lessons Learned: Interactions and Constraints

Determining the best implementation of the interactions and constraints is a central challenge to the application of Abaqus to folded deployable structures. First, consider the constraints. The initial approach concept strove to represent the panels as rigid bodies to reduce the computational complexity of the simulation. However, the interconnected nature of the panels proved to make this infeasible using the Abaqus framework. The primary way to connect the panels would be through either constraints or connector elements. A tie constraint between the mesh nodes of the edge of the panel can represent this behavior if the rotational degrees of freedom are not included in the constraint between the nodes. This is the method used in this analysis. However, Abaqus is not capable of enforcing a tie constraint between two rigid bodies. The rigid-body tools have been developed to represent interactions between test coupons and their fixtures, and therefore are not well suited to create this kind of model. Therefore, the panels are represented by deformable parts and are given accurate material properties to capture the real system's flexibility. The tape springs are attached to the hinge attachment plates using a surface-to-surface tie constraint between the overlapping surfaces. Finally, the hinge attachment plates are constrained to the panels at their attachment points using coupling constraints. Coupling constraints require that a set of slave nodes follow the behavior of a master point. The master point is set to a reference point on the hinge plates. In the full assembly, each panel is subject to either a master or slave tie constraint designation for the fold line. This reduces the available nodes for the slave nodes, and therefore a small radius of influence (set to 60 mm) is dictated for the coupling constraint slave node designation. A summary of all constraints needed to capture the prototype Miura unit structure is provided in Table 9.

Considering the interactions, there are a few primary concerns to address. These are all due to the presence of contact in the stowed step of the simulation. Obtaining the stowed configuration requires the tape springs contact with the attachment plates while not self-intersecting when they are brought together in the final configuration. Additionally, the shell representations of the panels may intersect in the fully stowed configuration. The panel contact interactions are considered negligible due to their thin shell designation, where at a full 180 deg fold, they would be occupying the same plane. Additionally, the expected behavior of the system does not include panel-to-panel contact through deployment. A basic "hard contact" property is defined for all contact interactions. Contact interactions are defined between each of the attachment plates and the tape

springs. These contact interactions are found to be a primary influence on the deployment behavior, where a hard contact definition results in a failed deployment, but a staged multistep defined separation results in the expected deployment behavior. No experiments were conducted to model this contact surface, and so these results must be taken with a grain of salt. Future work must be careful in modeling any contact surfaces within the structure. Additionally, self-contact interactions are defined for the tape springs to prevent self-intersection in the fully deployed configuration. A general self-contact designation for the full model is not used because it is unnecessary and computationally infeasible.

4. Lessons Learned: Loads and Boundary Conditions

To obtain the free-deployment dynamics behavior, the system must first be preloaded into the high strain initial condition and then released for deployment. The loads and boundary conditions modules provide tools to manipulate the model into the desired initial conditions for the dynamic analysis. The limitations of the software require this to be a multistep process. The specific sequential implementation of these loads and boundary conditions is outlined in the next section. The first boundary condition fixes the position of the P4 panel by applying encastre boundary conditions at each of the reference points of the hinge attachment plates. These plates are selected because the rigid bodies control both the panel behavior and the tape spring behaviors. Similarly, the primary fold-enforcing boundary condition is applied at the hinge attachment plate Reference Points (RPs) that are mounted to the P3 panel. A small initial fold is introduced to the 2-1 hinge fold line to ensure the fold starts in the correct direction but is otherwise uncontrolled. The boundary conditions of the static general analysis are applied over a linear ramp on an arbitrary time step, and simultaneously controlling more than one fold line is not recommended over the full course of the folding step. Additionally, a loading condition is applied to the tape springs to help initialize the folding behavior. This is a pressure load applied uniformly across the tape springs to press them flat against the panels at the initial fold. This is necessary because of the high stiffness condition of the tapes close to the initial buckling in folding. After the initial fold, the pressure is reduced for the duration of the folding. After folding, the pressure is deactivated. All boundary conditions and loads are summarized in Tables 10 and 11, and they are removed for the free-deployment step. The initial conditions enforced in Abaqus are not the same as the measured boundary conditions using this preloading approach, and Abaqus was unable to converge to those initial conditions with further iteration. However, the idealized initial conditions of the Abaqus simulation are close enough to simulate the deployment.

5. Lessons Learned: Step Sequence

The step sequence is outlined in detail in Table 12 and references the same loads and boundary conditions defined in Tables 10 and 11. The complexity of the multistep approach to creating the desired preloaded condition of this structure illustrates the difficulty of this approach for folded deployable spacecraft structures. This prototype only contains one fold pattern unit structure and is the minimum

Table 9   Abaqus model constraint definitions

Constraint	Type	Master	Slave
H21	Tie	Panel 2 edge nodes	Panel 1 edge nodes
H32	Tie	Panel 3 edge nodes	Panel 2 edge nodes
H14	Tie	Panel 1 edge nodes	Panel 4 edge nodes
P3-hinge 1	Kinematic coupling	Hinge plate 1	Panel 3
P3-hinge 2	Kinematic coupling	Hinge plate 2	Panel 3
P4-hinge 3	Kinematic coupling	Hinge plate 3	Panel 4
P4-hinge 4	Kinematic coupling	Hinge plate 4	Panel 4
Tape 1-hinge 1	Tie	Hinge plate 1	Tape spring 1
Tape 1-hinge 2	Tie	Hinge plate 2	Tape spring 1
Tape 2-hinge 3	Tie	Hinge plate 3	Tape spring 2
Tape 2-hinge 4	Tie	Hinge plate 4	Tape spring 2

Table 10   Abaqus model boundary conditions

Boundary condition	Type	Location
P4	Encastre	RPs on P4 rigid bodies
P3	Rotation	RPs on P3 rigid bodies
h21 nodes	Rotation	Fold line nodes on h21

Table 11   Abaqus model load conditions

Parameter	Value
Load condition	Press tapes
Type	Pressure
Location	Tape spring surfaces

Table 12   Abaqus model step specifications

Step	BC P4	BC P3	BC H21	BC adjust	Press tapes
Initial	——	——	——	——	——
Initial fold	Encastre	$\begin{bmatrix} - & 0 & 0 & 0 & 0.1 & 0 \end{bmatrix}$	UR2 = 0.1	——	2000
Full fold	Encastre	$\begin{bmatrix} - & 0 & - & 0 & 3 & 0 \end{bmatrix}$	Inactive	——	1000
Release press	Encastre	$\begin{bmatrix} - & 0 & - & 0 & 3 & 0 \end{bmatrix}$	Inactive	——	Inactive
Deploy	Encastre	Inactive	Inactive	Inactive	Inactive

BC = boundary condition, UR = rotational displacement.
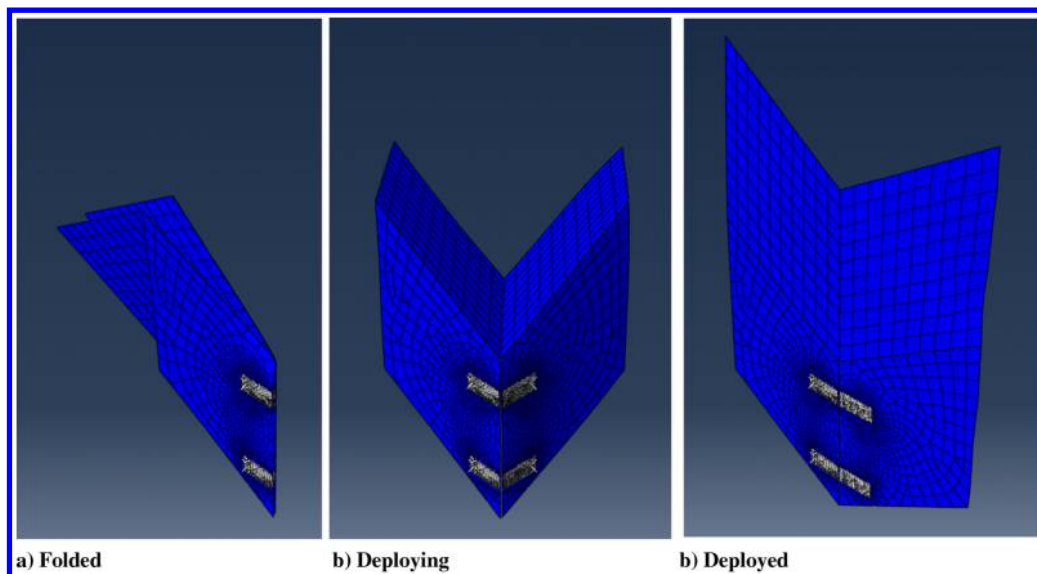
Fig. 21   Graphic representation of the deployment stages from the Abaqus simulation graphic user interface. A video is available in the Supplemental Material.

pattern case where, in practice, tens to hundreds of unit structures are desired. The analysis clock time for the preloaded condition steps is 45 min.

### B. Abaqus Deployment Trial Results and Comparison to Measured Tests

The Abaqus/Explicit deployment simulation results are displayed over the experimental deployment data in Fig. 22, and they show the bulk deployment behavior is well predicted. Two seconds of simulation requires approximately 22 h of user clock time to compute using Windows 10 on a Parallels virtual machine with 4 GB of memory and two processors. The clock time can be significantly improved with more advanced computer hardware. Additionally, an optimization study to provide a refined mesh may improve the simulation time. Looking at the secondary behaviors, such as the oscillations and motion trends, it is possible the discrepancies between the experimental and Abaqus simulations are due to test environment effects, such as atmospheric drag and gravity. Although these effects can be simulated in Abaqus, this is not done due to challenges with defining the relative orientation of these effects. The predicted deployment time is seen to be 0.88 s, midway between the cup-up and cup-down trials. The result is suspected to be due to the initial conditions of the simulation, as well as the imperfect modeling of the contact behavior between the tape springs and their attachment plates. Overall, the simulation is able to predict the bulk behaviors and the settling of the structure in the deployed state well, where the initial oscillations appear to settle out over 1 s in both the Abaqus simulation and the experimental data (see Fig. 22).

This Abaqus modeling effort quantifies the time and effort commitment of creating a high-fidelity deployment model, and it highlights the limitations of the multibody dynamics modeling

approach. In practice, it is recommended that the multibody modeling approach be implemented for large-scale fold patterns of many bodies and for early design iterations of the geometry, mass, and hinge properties. The fast computation speed of the multibody framework increases feasibility of large parameter design studies, and the accuracy of the deployment model is shown to be sufficient for informing early design evaluations. A high-fidelity FEA deployment model should also be studied, but it is primarily recommended for validation phases of the project. The FEA model is best able to capture the secondary behaviors of the flexible panels, the lockout of the hinges, and contact behaviors. Deployment testing of a prototype provides context for expected performance and should be conducted during the design cycle of the project. All three datasets confirm the prototype folded structure will successfully self-deploy with the tape spring actuated hinge design.

VII.   Conclusions

In this paper, simulations of a self-actuated origami-folded prototype structure are constructed from complex hinge models integrated into a multibody dynamics model of the prototype. The simulations are compared to experimental deployment dynamics data, and performance is evaluated. The simulations of both 1-DOF and 4-DOF hinge models show good prediction of the deployment time; however, deployment behavior past the peak deployment is not well predicted due to constraint violations and a lack of contact and damping in the model. Issues due to constraint violations are identified as the primary challenge of accurate deployment dynamics modeling for free-deploying high strain structures. An additional simulation is constructed using a full finite element analysis, and the deployment time is also well predicted, as well as the settling
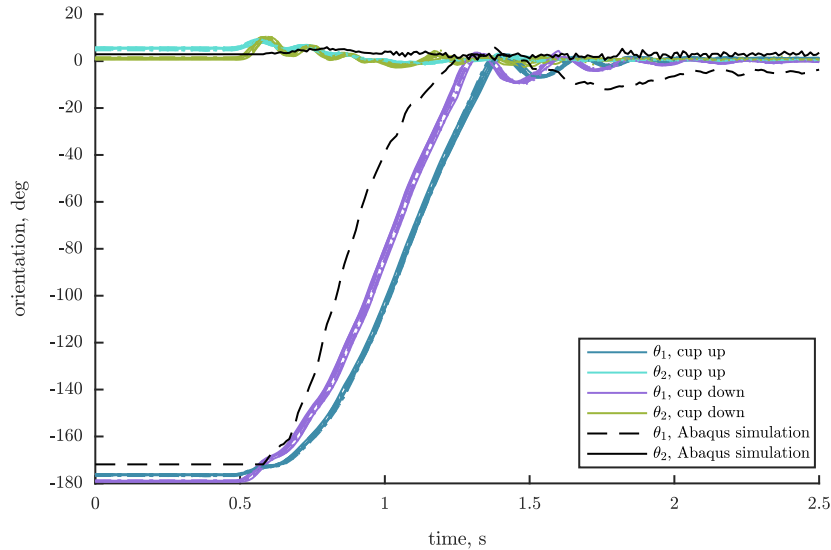
a) **Hinge 4-3 orientations**
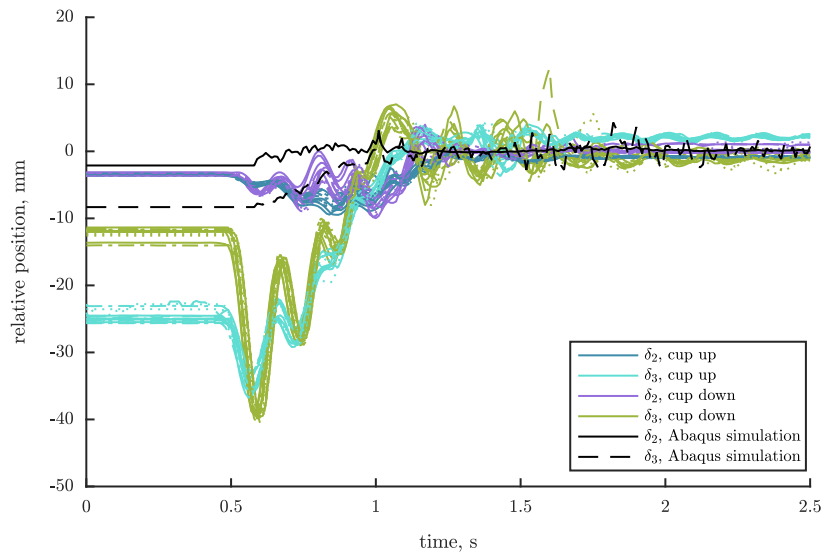
b) **Hinge 4-3 positions**

Fig. 22   Deployment actuation predictions from the Abaqus FEA model of the four states of hinge 4-3 and their experimental counterparts from all trials.

period. The overall deployment behavior is also captured across multiple degrees of freedom; however, the simulation takes 22 h of computation time to complete, as compared to 6–7 s for the multibody dynamics models. This confirms the original motivation of designing a more computationally efficient method of deployment dynamics modeling, and it demonstrates that multibody dynamics modeling is able to predict some deployment behavior with similar accuracy. In practice, it is recommended that the multibody modeling approach be implemented for large-scale fold patterns of many bodies and for early design iterations of the geometry, mass, and hinge properties. The fast computation speed of the multibody framework increases feasibility of large parameter design studies, and the accuracy of the deployment model is shown to be sufficient for informing early design evaluations. The FEA model is best able to capture the secondary behaviors of the flexible panels, the lockout of the hinges, and contact behaviors. Deployment testing of a prototype provides context for expected performance and should be conducted during the design cycle of the project. All three datasets confirm the prototype folded structure will successfully self-deploy with the tape spring actuated hinge design, demonstrating the feasibility of implementing this novel design concept.

Appendix: Nonlinear Regression Coefficients

Table A1   Equal- and opposite-sense nominal fold nonlinear regression coefficients

Parameter	Value
a_2	2.24e − 2
a_3	1.43e − 2
a_4	0
a_5	−18.54
a_6	−3.43
b_1	−21.26
b_2	4.08
b_3	0.16
b_4	−1.62e − 4
c_1	−3.10e − 5
c_2	1.02e − 5

Table A2   Reduced coefficients for the prototype hinge assembly FEA model

Coefficient	M_{0_2}	M_{0_3}	N_{0_1}	N_{0_2}	N_{0_3}
a_1	105.29e − 3	−69.86	−129.75e − 3	−768.48e − 3	723.68e − 3
a_2	−318.17e − 3	−123.21e − 3	207.75	−94.46	173.97
a_3	−18.99e − 3	−207.82e − 3	−890.34	288.94	−528.02
a_4	22.12e − 3	15.40e − 3	60.89	−4.33	3.10
a_5	7.75	14.29	−7.19e − 3	151.34e − 3	−164.95e − 3
a_6	−17.48	−32.86	−23.56e − 3	−334.97e − 3	333.49e − 3
$b_{1,1}$	91.77	34.04	−109.58e − 3	343.78e − 3	−599.31e − 3
$b_{2,2}$	−4.20e − 6	−3.60e − 6	−2.08e − 3	1.25e − 3	−1.97e − 3
$b_{3,3}$	−1.83e − 6	−1.71e − 6	−481.68	557.51	−1.07e − 3
$b_{4,4}$	−15.33e − 3	−13.44e − 3	−5.83	3.59	−5.80
$b_{5,5}$	216.17e − 3	−11.03e − 3	178.22e − 6	656.73e − 6	4.58e − 3
$b_{6,6}$	208.16e − 3	−104.07e − 3	61.87e − 6	1.41e − 3	2.54e − 3
$b_{1,2}$	−198.66e − 3	−105.69e − 3	−292.91	61.40	−89.76
$b_{1,3}$	6.30e − 3	−95.52e − 3	−397.31	133.37	−248.77
$b_{1,4}$	10.26e − 3	5.02e − 3	27.98	−2.49	500.11e − 3
$b_{1,5}$	−7.34	418.17e − 3	547.87e − 6	−5.14e − 3	−49.82e − 3
$b_{1,6}$	−707.44e − 3	−15.65	−18.69e − 3	−143.05e − 3	85.93e − 3
$b_{2,3}$	5.46e − 6	4.99e − 6	2.03e − 3	−1.31e − 3	2.34e − 3
$b_{2,4}$	497.43e − 3	431.36e − 3	220.90	−127.77	200.22
$b_{2,5}$	6.37e − 3	2.49e − 3	9.77	−3.78	5.16
$b_{2,6}$	12.70e − 3	14.99e − 3	18.64	−3.34	7.30
$b_{3,4}$	−342.40e − 3	−314.80e − 3	−106.69	85.12	−157.63
$b_{3,5}$	−2.15e − 3	−288.38	−7.46	−480.06e − 3	1.35
$b_{3,6}$	−2.42e − 3	−2.48e − 3	1.55	−1.22	1.84
$b_{4,5}$	−251.78	−13.29	−601.34e − 3	65.04e − 3	80.53e-3
$b_{4,6}$	−644.11	−698.39	−384.07e − 3	89.92e − 3	−219.37e − 3
$b_{5,6}$	−334.05e − 3	395.28e − 3	812.43e-6	2.64e − 3	−1.33e − 3

Table A3   Equal-sense primary fold model nonlinear regression coefficients with asymmetric configuration data[a]

Parameter	Value
a_2	194.77
a_3	120.18
a_4	0
a_5	−14.78
a_6	−2.66
b_1	−23.93
b_2	3.70
b_3	0.15
b_4	−1.50e − 4

[a]Coefficients have units of newtons per millimeter in this table.

Acknowledgments

References

[1] Zirbel, S. A., Trease, B. P., Thomson, M. W., Lang, R. J., Magleby, S. P., and Howell, L. H., "HanaFlex: A Large Solar Array for Space Applications," *Micro- and Nanotechnology Sensors, Systems, and Applications VII*, edited by T. George, A. K. Dutta, and M. S. Islam, Vol. 9467, SPIE, Bellingham, WA, 2015, pp. 179–187.
https://doi.org/10.1117/12.2177730

[2] Murphy, D., "MegaFlex—The Scaling Potential of UltraFlex Technology," *53rd AIAA/ASME/ASCE/AHS/ASC Structures, Structural Dynamics and Materials Conference*, AIAA Paper 2012-1581, 2012.
https://doi.org/10.2514/6.2012-1581

[3] Jeon, S. K., and Footdale, J. N., "Scaling and Design of a Modular Origami Solar Array," *AIAA SciTech Spacecraft Structures Conference*, AIAA Paper 2018-2204, 2018.

[4] Jeon, S., and Murphey, T., "Fundamental Design of Tensioned Precision Deployable Space Structures Applied to an X-Band Phased Array," *53rd AIAA/ASME/ASCE/AHS/ASC Structures, Structural Dynamics and Materials Conference*, AIAA Paper 2012-1447, 2012.
https://doi.org/10.2514/6.2012-1447

[5] Pehrson, N. A., and Banik, J., "Folding Approaches for Tensioned Precision Planar Shell Structures," *AIAA SciTech Spacecraft Structures Conference*, AIAA Paper 2018-1439, 2018.

[6] Thomson, M., Lisman, D., Helms, R., Walkemeyer, P., Kissil, A., Polanco, O., and Lee, S.-C., "Starshade Design for Occulter Based Exoplanet Missions," *Space Telescopes and Instrumentation 2010: Optical, Infrared, and Millimeter Wave*, Vol. 7731, SPIE Proceedings, 2010.

[7] Reynolds, W., Jeon, S., and Banik, J., "Advanced Folding Approaches for Deployable Spacecraft Payloads," *Proceedings of the ASME 2013 International Design Engineering Technical Conference and Computers and Information in Engineering Conference*, ASME, New York, 2013.

[8] Kling, D., Jeon, S., and Banik, J., "Novel Folding Methods for Deterministic Deployment of Common Space Structures," *3rd AIAA Spacecraft Structures Conference*, AIAA Paper 2016-2168, 2016.

[9] Zirbel, S. A., Trease, B., Magleby, S. P., and Howell, L. L., "Deployment Methods for an Origami-Inspired Rigid-Foldable Array," *Proceedings of the 40th Aerospace Mechanisms Symposium*, NASA Goddard Space Flight Center, May 2014, pp. 189–194.

[10] Huffman, D. A., "Curvature and Creases: A Primer on Paper," *IEEE Transactions on Computers*, Vol. c-25, No. 10, 1976, pp. 1010–1019.

[11] Woo, K., and Jenkins, C. H., "Effect of Crease Orientation on Wrinkle–Crease Interaction for Thin Membranes," *Journal of Spacecraft and Rockets*, Vol. 50, No. 5, 2013, pp. 1024–1034.
https://doi.org/10.2514/1.A32183

[12] Murphey, T. W., and Pellegrino, S., "A Novel Actuated Composite Tape-Spring for Deployable Structures," *45th AIAA/ASME/ASCE/AHS/ASC Structures, Structural Dynamics and Materials Conference*, AIAA Paper 2004-1528, 2004.

[13] Pellegrino, S., *Deployable Structures*, Springer-Verlag, Berlin, 2001.

[14] Fulton, J., and Schaub, H., "Dynamic Modeling of Folded Deployable Space Structures with Flexible Hinges," *2017 AAS/AIAA Astrodynamics Specialist Conference*, AAS Paper 17-747, 2017.

[15] Fulton, J., and Schaub, H., "Closed-Chain Forward Dynamics Modeling of a Four-Panel Folding Spacecraft Structure," *International Astronautical Congress*, Paper IAC-18.C1.4.3x42523, 2018.

[16] Fulton, J., and Schaub, H., "Non-Symmetric Behavior of High Strain Composite Tape Spring Hinges for Folding Structures," *Spacecraft Structures Conference, AIAA SciTech Forum*, AIAA Paper 2019-1747, 2019.

[17] Fulton, J., and Schaub, H., "Forward Dynamics Algorithm for Origami-Folded Deployable Spacecraft Structures," *International Astronautical Congress*, Paper IAC-19.C1.5.8x50478, 2019.

[18] Sauder, J., Chahat, N., Hodges, R. E., Peral, E., Rahmat-Samii, Y., and Thomson, M., "Lessons Learned from a Deployment Mechanism for a Ka-Band Deployable Antenna for CubeSats," *Proceedings of the 44th Aerospace Mechanisms Symposium*, NASA Glenn Research Center, May 2018, pp. 361–373.

[19] Footdale, J. N., and Banik, J., "Design and Deployment Testing of the Multi-Arm Radial Composite (MARCO) Reflector Antenna," *3rd AIAA Spacecraft Structures Conference*, AIAA Paper 2016-0700, 2016.
https://doi.org/10.2514/6.2016-0700

[20] Fulton, J., Jeon, S., and Murphey, T. W., "Flight Qualification Testing of a Meter-Class CubeSat Deployable Boom," *4th AIAA Spacecraft Structures Conference*, AIAA Paper 2017-0621, 2017.

[21] Mobrem, M., and Adams, D. S., "Deployment Analysis of the Lenticular Jointed Antennas Onboard the Mars Express Spacecraft," *Journal of Spacecraft and Rockets*, Vol. 46, No. 2, 2009, pp. 394–402.

[22] Adams, D., and Mobrem, M., "MARSIS Antenna Flight Deployment Anomaly and Resolution," *47th AIAA/ASME/ASCE/AHS/ASC Structures, Structural Dynamics, and Materials Conference*, AIAA Paper 2006-1684, 2006.
https://doi.org/10.2514/6.2006-1684

[23] Montazersadgh, F., and Mobrem, M., "Structural Analysis Methodology for Space Deployable Structures Using Multi-Body Dynamic Analysis Solver," *AIAA Modeling and Simulation Technologies Conference*, AIAA Paper 2018-0421, 2018.

[24] Olson, G., Murphey, T., and Thomas, G., "Free Deployment Dynamics of a Z-Folded Solar Array," AIAA Paper 2011-1730, 2011.
https://doi.org/10.2514/6.2011-1730

[25] Pehrson, N. A., Smith, S. P., Ames, D. C., Magleby, S. P., and Arya, M., "Self-Deployable, Self-Stiffening, and Retractable Origami-Based Arrays for Spacecraft," *AIAA SciTech Spacecraft Structures Conference*, AIAA Paper 2019-0484, 2019.

[26] Blandino, J. R., Ross, B., Woo, N., Smith, Z., and McNaul, E., "Simulating CubeSat Structure Deployment Dynamics," *AIAA SciTech Spacecraft Structures Conference*, AIAA Paper 2018-1677, 2018.

[27] Tachi, T., "Rigid-Foldable Thick Origami," Vol. 5, *5th International Meeting of Origami Science, Mathematics, and Education*, Singapore Management Univ., CRC Press, July 2010.
https://doi.org/10.1201/b10971-24

[28] Ku, J. S., and Demaine, E. D., "Folding Flat Crease Patterns with Thick Materials," *Journal of Mechanisms and Robotics*, Vol. 8, No. 3, March 2016, Paper 031003.
https://doi.org/10.1115/1.4031954

[29] Arya, M., Lee, N., and Pellegrino, S., "Crease-Free Biaxial Packaging of Thick Membranes with Slipping Folds," *International Journal of Solids and Structures*, Vol. 108, March 2017, pp. 24–39.
https://doi.org/10.1016/j.ijsolstr.2016.08.013

[30] Hernandez, H., Hartl, D. J., and Lagoudas, D. C., "Modeling and Design of Shape Memory Alloy-Based Origami Structures with Smooth Folds," *AIAA SciTech Conference*, AIAA Paper 2017-1875, 2017.

[31] Seffen, K. A., and Pellegrino, S., "Deployment Dynamics of Tape Springs," *Proceedings of the Royal Society of London, Series A: Mathematical and Physical Sciences*, Vol. 455, No. 1983, March 1999, pp. 1003–1048.

[32] Soykasap, O., "Analysis of Tape Spring Hinges," *International Journal of Mechanical Sciences*, Vol. 49, 2007, pp. 853–860.

[33] Walker, S. J. I., and Aglietti, G., "Study of the Dynamics of Three-Dimensional Tape Spring Folds," *AIAA Journal*, Vol. 42, No. 4, 2004, pp. 850–856.

[34] Jain, A., *Robot and Multibody Dynamics*, Springer Science+Business Media, Berlin, 2011, pp. 35–40, 123–131.

V. Babuska
Associate Editor